Selective adsorption and separation of pyridine and picoline using hybrid[3]arene-based nonporous adaptive crystals

Xueyu Zhu,[a] Miaomiao Yan,[a] Yuanxin Zhang,[a] Jingyu Chen,[a] Haoze Zhu,[a] Yuyue Chi,[a] Yuan Yu[b] and Jiong Zhou*[a]

[a]*Department of Chemistry, College of Sciences, Northeastern University, Shenyang 110819, P. R. China. E-mail: zhoujiong@mail.neu.edu.cn*

[b]*School of Materials and Energy, University of Electronic Science and Technology of China, Chengdu 610054, P. R. China.*

Electronic Supplementary Information (38 pages)

1. *Materials*

All chemicals including 2-picoline (**2-PC**), 3-picoline (**3-PC**), 4-picoline (**4-PC**) and pyridine (**Py**) were purchased and used as received. Hybrid[3]arene (**H**) was synthesized as described previously.[1] Activated crystalline **H** was referred to as **H***α*. **H***α* were prepared according to reported procedure.[2]

2. Methods

2.1. Solution ^{1}H NMR

Solution ^{1}H NMR spectra were recorded at 400 MHz using a Bruker Avance 400 NMR spectrometer.

2.2. Powder X-ray diffraction

Powder X-ray diffraction (PXRD) data were collected on a Rigaku Ultimate-IV X-ray diffractometer operating at 40 kV/40 mA using the Cu K*α* line (λ = 1.5418 Å). Data were measured over the range of 4−40° in 5°/min steps over 8 min.

2.3. Thermogravimetric analysis

Thermogravimetric analysis (TGA) was carried out using a Q5000IR analyzer (TA Instruments) with an automated vertical overhead thermobalance. The samples were heated at 10 °C/min using N_2 as the protective gas.

2.4. Single crystal growth

Single crystals of **2-PC**-loaded **H**, **3-PC**-loaded **H**, **4-PC**-loaded **H**, or **Py**-loaded **H** were grown by slow evaporation: 2 mg of dry **H***α* powders were put in a small vial where 1 mL of **2-PC**, **3-PC**, **4-PC**, or **Py** was added. Adding dichloromethane until all **H***α* powders were dissolved. The resultant transparent solution was allowed to evaporate slowly to give nice crystals in 2 to 3 days.

2.5. Single crystal X-ray diffraction

Single crystal X-ray diffraction data were collected on a Bruker D8 VENTURE CMOS X-ray diffractometer with graphite monochromatic Cu K*α* radiation (λ = 1.54178 Å).

2.6. Head space gas chromatography

Head space gas chromatography (HS-GC) analysis: HS-GC measurements were

carried out using an Agilent 7890B instrument configured with a FID detector and a DB-624 column (30 m × 0.53 mm × 3.0 μm). Samples were analyzed using headspace injections and were performed by incubating at 100 °C for 10 min followed by taking 1 mL of the headspace. The following GC method was used: the oven was programmed from 50 °C, and ramped in 10 °C min^{-1} increments to 150 °C with 15 min hold; the total run time was 25 min; the injection temperature was 250 °C; the detector temperature was 280 °C with nitrogen, air, and make-up flow rates of 35, 350 and 35 mL min^{-1}, respectively; the helium (carrier gas) flow rate was 3.0 mL min^{-1}. The samples were injected in the split mode (30:1).

2.7. Theoretical calculations

All calculations were performed by density functional theory (DFT) using the B3LYP/def2-TZVP(-f)[3,4] basis set under ORCA 5.0.4.[5] Independent gradient model based on Hirshfeld partition (IGMH) analysis was carried out by Multiwfn 3.6 program through function 20 (visual study of weak interaction) and visualized by Visual Molecular Dynamics software.[6] Multiwfn combined with VMD was used to analyze and plot the electrostatic potential distribution on the molecular surface. The thermodynamic parameters of **H**α for **2-PC**, **3-PC**, **4-PC**, **Py** were calculated according to the following formula: $\Delta G = G_{HOST-GUEST} - G_{HOST} - G_{GUEST}$ and $\Delta H = H_{HOST-GUEST} - H_{HOST} - H_{GUEST}$. The Shermo 2.6 program was used to process thermodynamic data.[7,8]

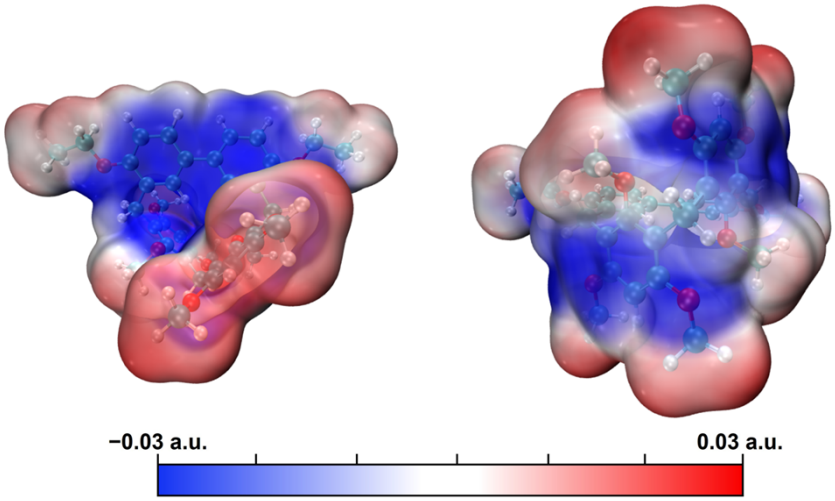

Scheme S1. ESP maps of **H** from different perspectives.

3. Crystallography data

Table S1. Experimental single crystal X-ray data for **2-PC@H** and **3-PC@H**

Formula	**2-PC@H**	**3-PC@H**
Crystallization solvent	2-picoline	3-picoline
Empirical formula	$C_{43}H_{49}O_8N$	$C_{43}H_{49}O_8N$
Formula weight	707.83	707.83
Temperature	273 K	273 K
Wavelength (Å)	1.54178	1.54178
Crystal system	triclinic	triclinic
Space group	*P*-1	*P*-1
a (Å)	10.812	10.763
b (Å)	13.298	13.376
c (Å)	15.639	15.636
α (°)	109.74	111.14
β (°)	97.43	97.45
γ (°)	107.36	107.23
Volume (Å^3)	11342.0(3)	1933.4
Z	2	2
Density (g·cm^{-3}) (calculated)	1.204	1.216
Absorption (mm^{-1}) coefficient	0.666	0.673
F(000)	756.0	756.0
Crystal size (mm^3)	0.12 × 0.1 × 0.08	0.12 × 0.1 × 0.08
2Θ range for data collection (°)	6.212 to 133.108	6.286 to 132.864
Reflections collected	6868	6726
Independent reflections	6868 [R_{int} = 0]	6726 [R_{int} = 0]
Data/restraints/parameters	6868/1/466	6726/54/478
CCDC	2365196	2365197

Table S2. Experimental single crystal X-ray data for **4-PC@H** and **Py@H**.

Formula	**4-PC@H**	**Py@H**
Crystallization solvent	4-picoline	pyridine
Empirical formula	$C_{43}H_{49}O_8N$	$C_{42}H_{47}O_8N$
Formula weight	707.83	693.81
Temperature	273 K	273 K
Wavelength (Å)	1.54178	1.54178
Crystal system	triclinic	monoclinic
Space group	*P*-1	$P2_1/c$
a (Å)	10.921	14.323
b (Å)	13.405	21.361
c (Å)	15.518	15.805
α (°)	110.75	90
β (°)	99.02	109.84
γ (°)	107.99	90.00
Volume ($Å^3$)	1927.7	4548.3
Z	2	4
Density ($g \cdot cm^{-3}$) (calculated)	1.219	1.013
Absorption (mm^{-1}) coefficient	0.675	0.564
F(000)	756.0	1480.0
Crystal size (mm^3)	0.12 × 0.1 × 0.08	0.12 × 0.1 × 0.08
2Θ range for data collection (°)	3.192 to 66.744	7.244 to 133.316
Reflections collected	6769	36297
Independent reflections	6769 [R_{int} = 0]	8014 [R_{int} = 0.0823]
Data/restraints/parameters	6769/0/478	8014/18/469
CCDC	2370763	2370420

*4. Characterization of **H**α*

Synthesis of hybrid[3]arene (**H**): To the solution of 4,4'-biphenol diethyl ether (2.42 g, 10.0 mmol) and 1,3,5-trimethoxybenzene (3.36 g, 20.0 mmol) in $CHCl_3$ (200 mL), paraformaldehyde (0.900 g, 30.0 mmol) and trifluoroacetic acid (TFA) (10.0 mL) were added. The mixture was refluxed for 30 min, and the progress was monitored by thin-layer chromatography. The mixture was cooled to room temperature, and an excess of saturated aqueous Na_2CO_3 was added to neutralize TFA. The organic phase was separated and the crude product was purified by column chromatography (petroleum ether/CH_2Cl_2, *v*/*v* 10:1 → 3:1) to get **H** as a white solid (1.67 g, 25%), mp: 305.5-306.5 °C.

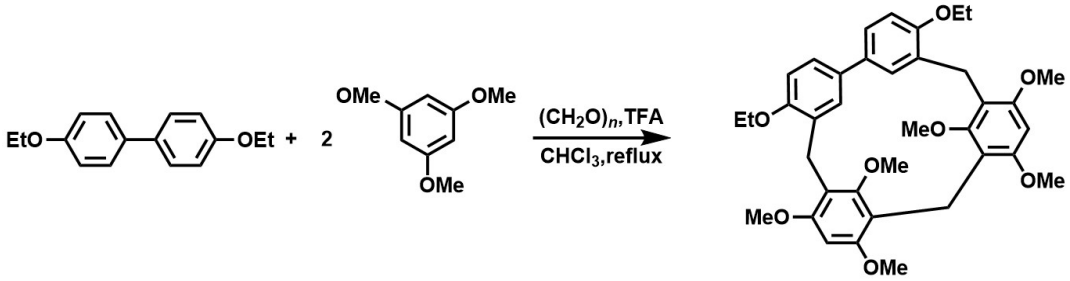

Scheme S2. Synthetic route to hybrid[3]arene (**H**).

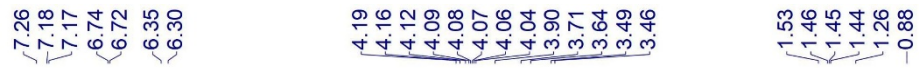

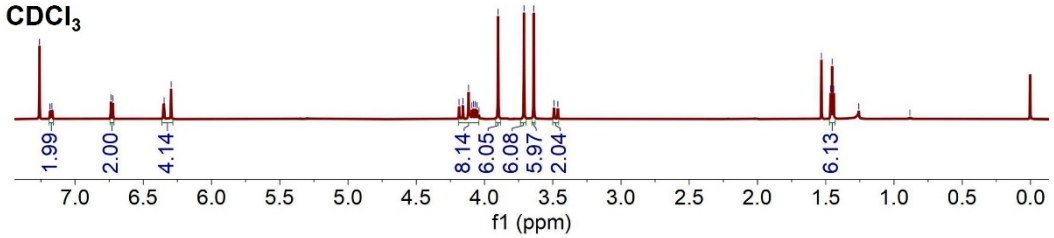

Figure S1. ^{1}H NMR spectrum (400 MHz, $CDCl_3$, 293 K) of **H**α.

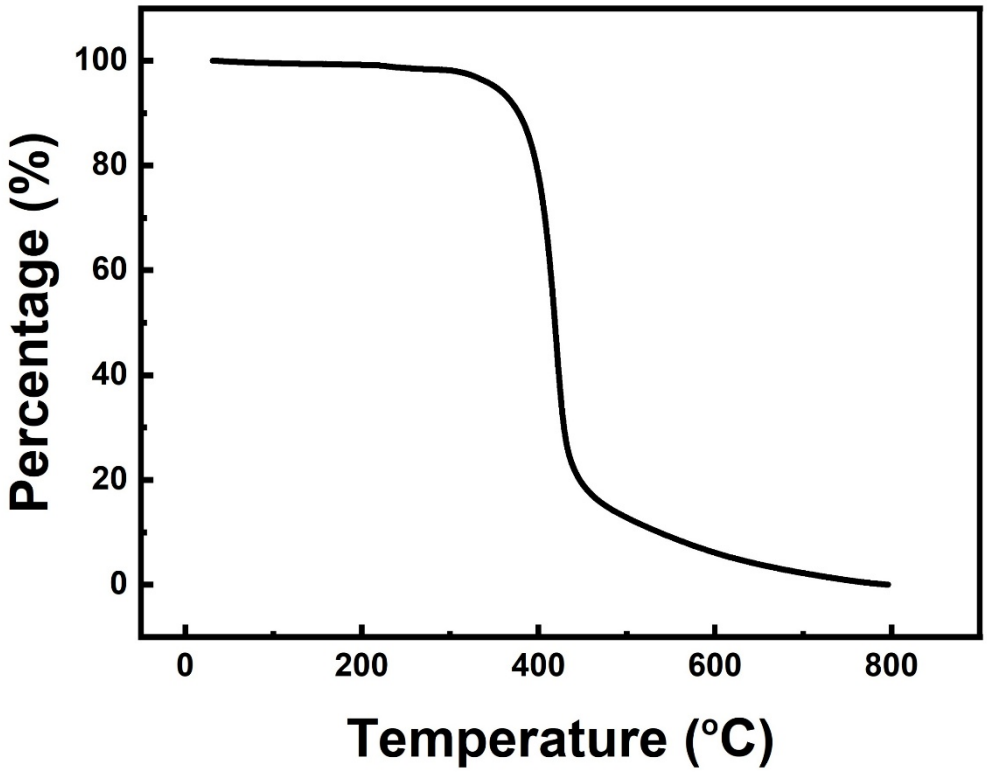

Figure S2. Thermogravimetric analysis of **H**α.

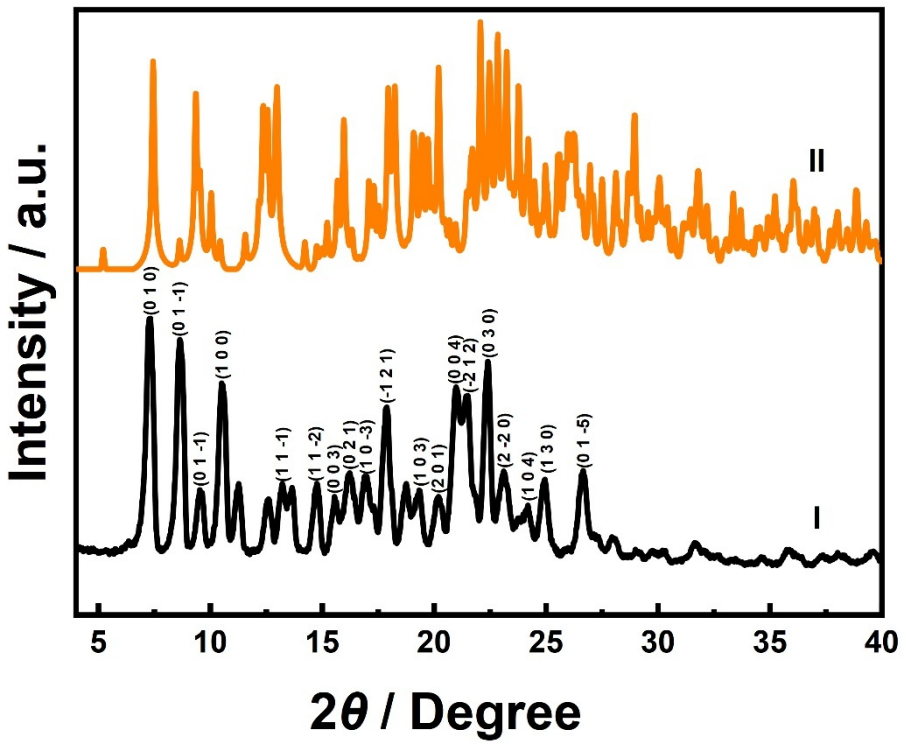

Figure S3. Powder X-ray diffraction pattern of **H**α: (I) original **H**α; (II) simulated from the single crystal structure of **H**.

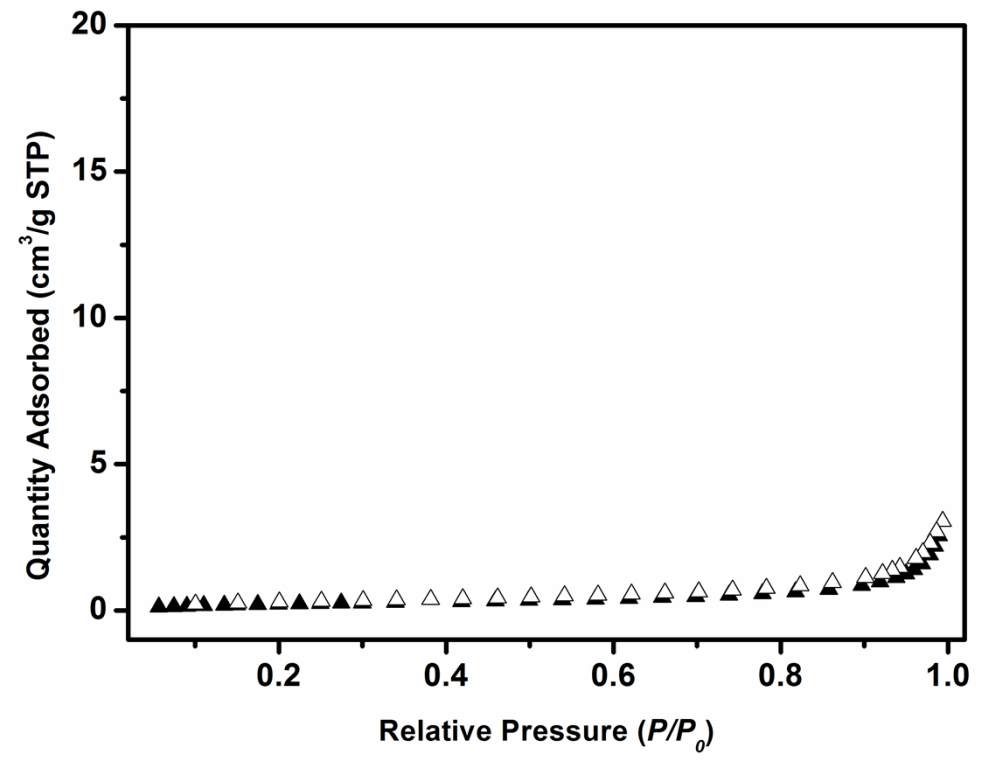

Figure S4. N_2 adsorption isotherm of **H***α*. The BET surface area value is 0.8995 m^2/g. Adsorption, closed symbols; desorption, open symbols.

*5. Single-component adsorption experiments of **H**α*

An open 5 mL vial containing 2.00 mg of guest-free **H***α* adsorbent was placed in a sealed 20 mL vial containing 0.5 mL of **Py**, **2-PC**, **3-PC**, or **4-PC**. Time-dependent solid–vapor adsorption plots of **H***α* were measured by completely dissolving the crystals and measuring the molar ratio of **Py**, **2-PC**, **3-PC**, or **4-PC** to **H** by ^{1}H NMR. Thermogravimetric analysis experiments were performed using **H***α* after vapor adsorption.

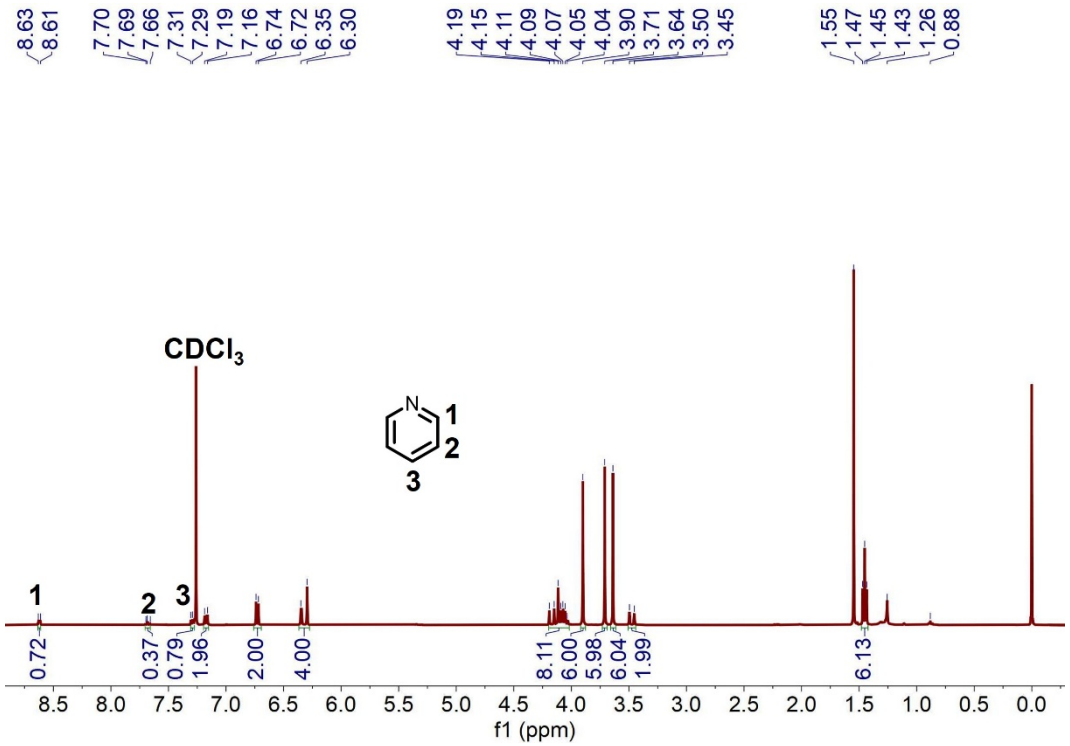

Figure S5. ^{1}H NMR spectrum (400 MHz, $CDCl_3$, 298 K) of **H***α* after adsorption of **Py** for 12 h.

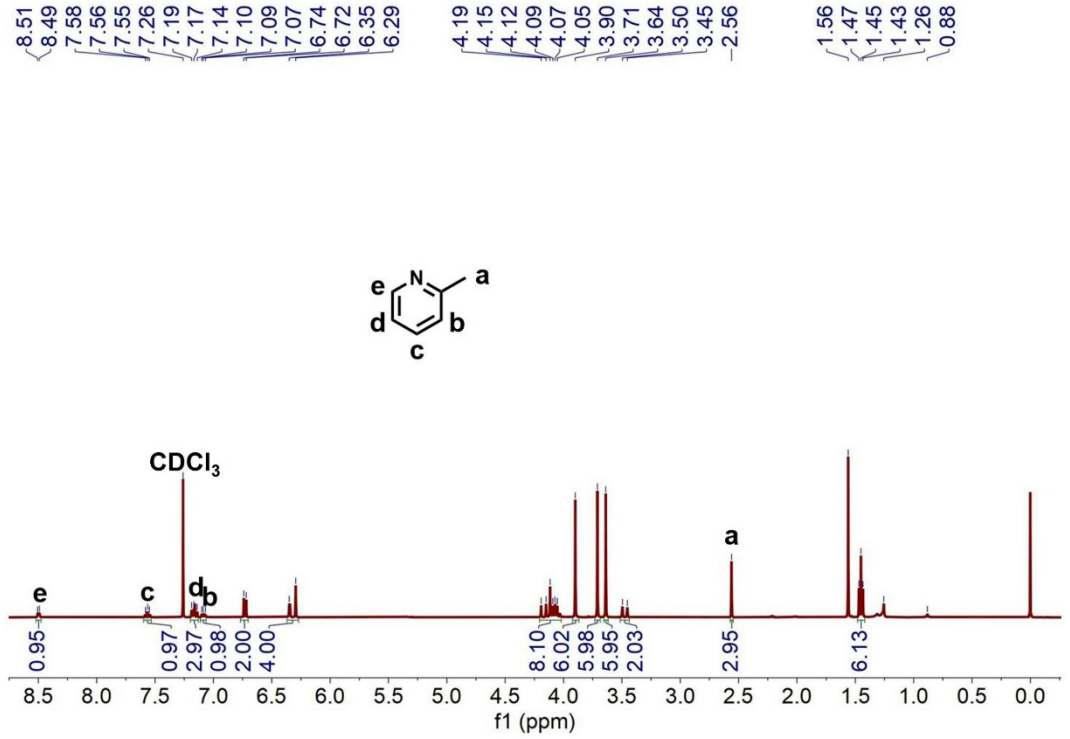

Figure S6. ^{1}H NMR spectrum (400 MHz, $CDCl_3$, 298 K) of **H***α* after adsorption of **2-PC** for 12 h.

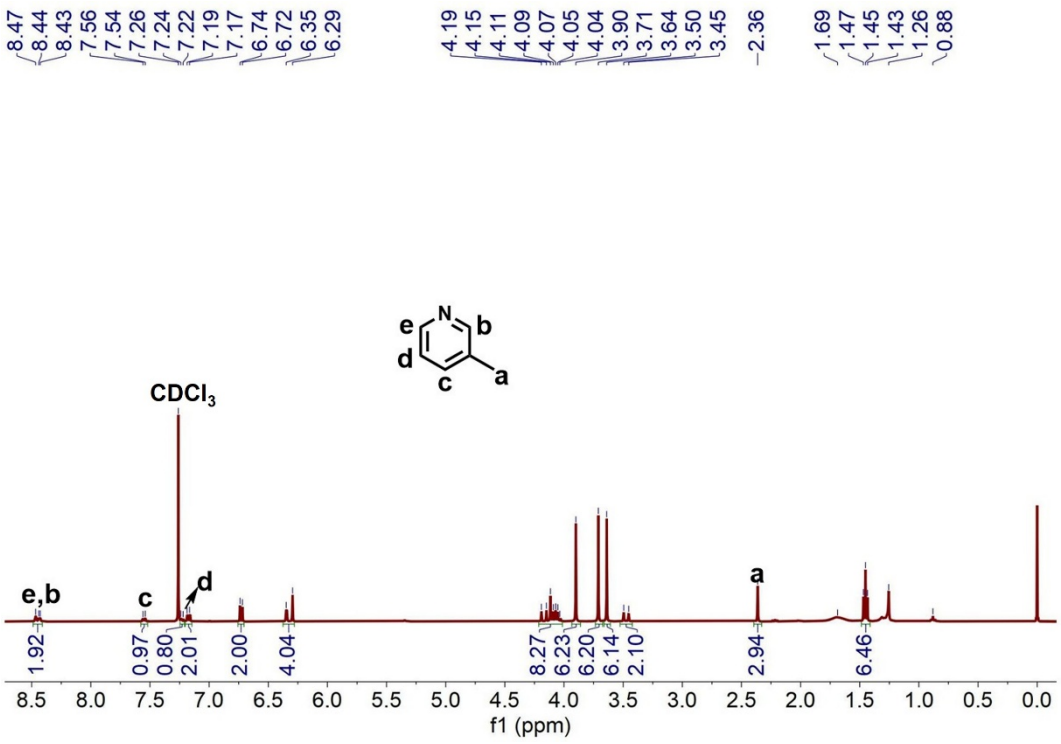

Figure S7. ^{1}H NMR spectrum (400 MHz, $CDCl_3$, 298 K) of **H***α* after adsorption of **3-PC** for 16 h.

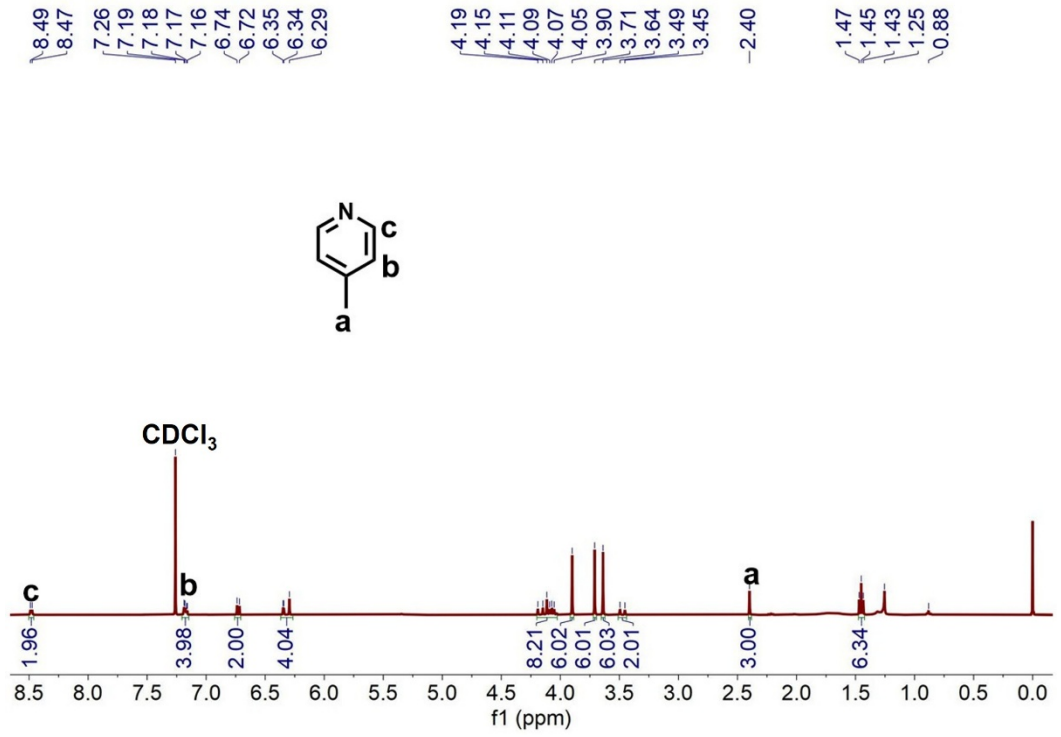

Figure S8. ^{1}H NMR spectrum (400 MHz, $CDCl_3$, 298 K) of **H***α* after adsorption of **4-PC** for 4 h.

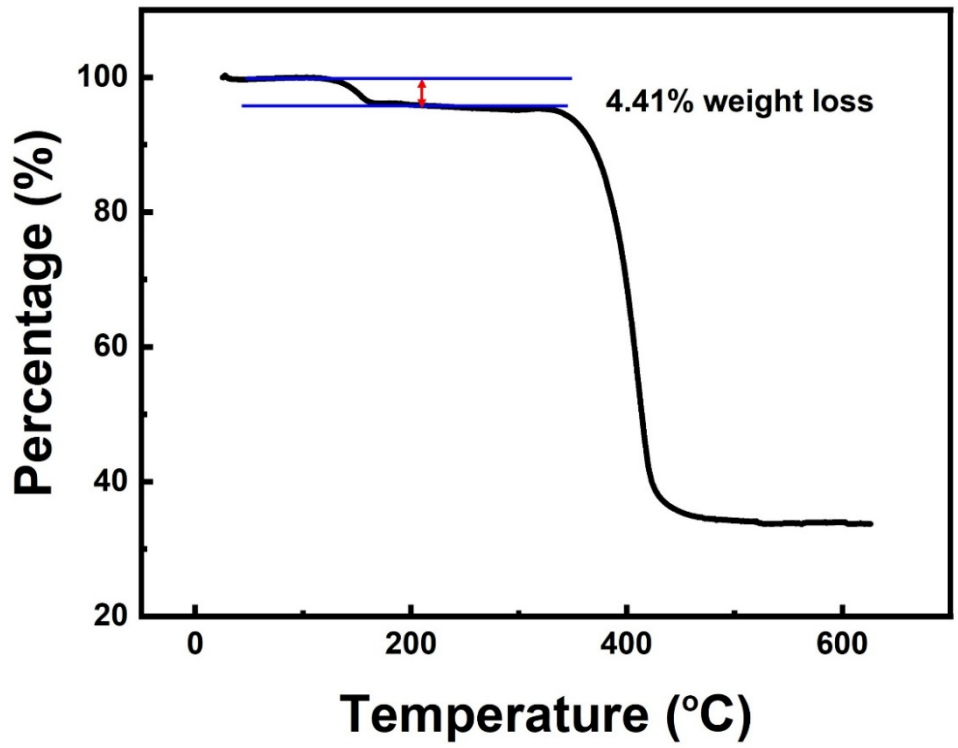

Figure S9. Thermogravimetric analysis of **H***α* after adsorption of **Py** for 12 h. The weight loss below 70 °C can be calculated as 0.36 **Py** molecule per **H***α* molecule.

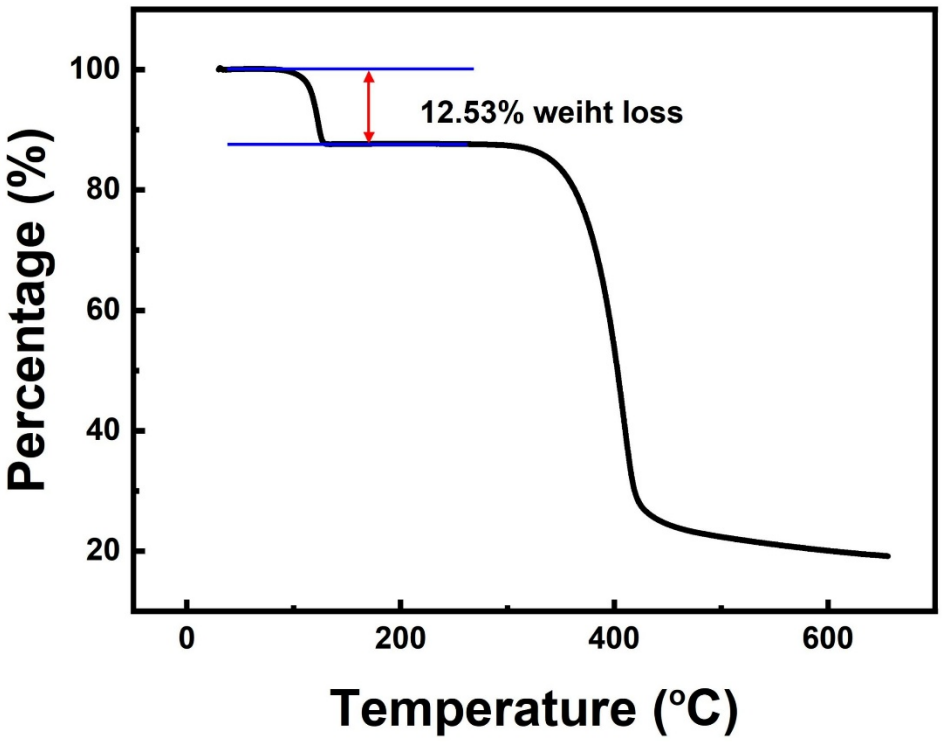

Figure S10. Thermogravimetric analysis of **H***α* after adsorption of **2-PC** for 12 h. The weight loss below 110 °C can be calculated as 0.94 **2-PC** molecule per **H***α* molecule.

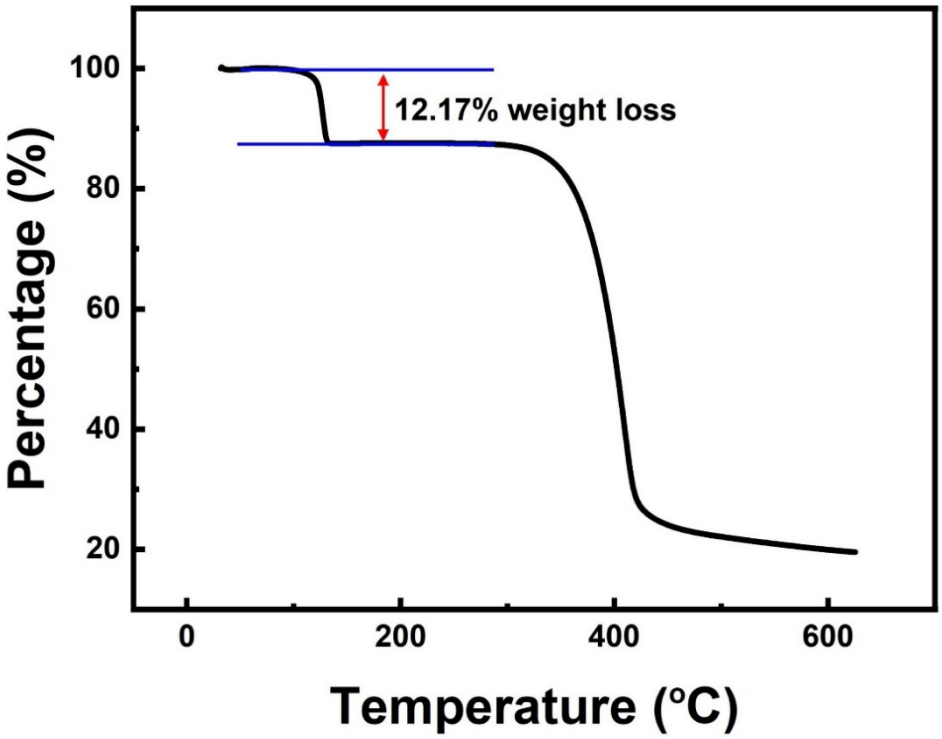

Figure S11. Thermogravimetric analysis of **H***α* after adsorption of **3-PC** for 16 h. The weight loss below 125 °C can be calculated as 0.91 **3-PC** molecule per **H***α* molecule.

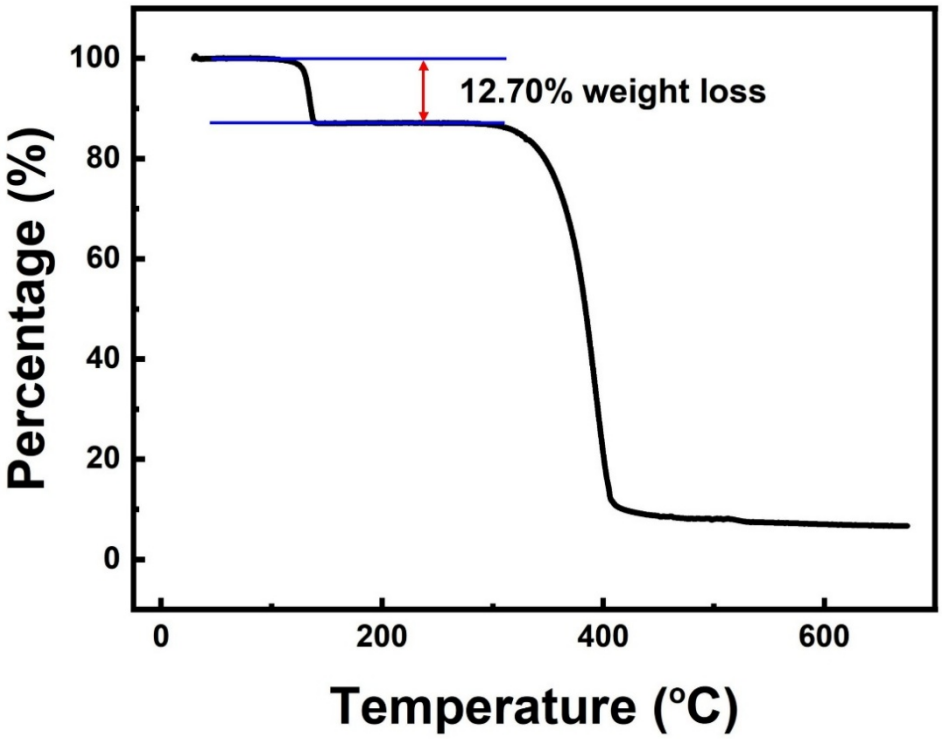

Figure S12. Thermogravimetric analysis of **H***α* after adsorption of **4-PC** vapor for 4 h. The weight loss below 130 °C can be calculated as 0.96 **4-PC** molecule per **H***α* molecule.

6. Noncovalent interactions analysis in single crystal structures of host–guest complexes

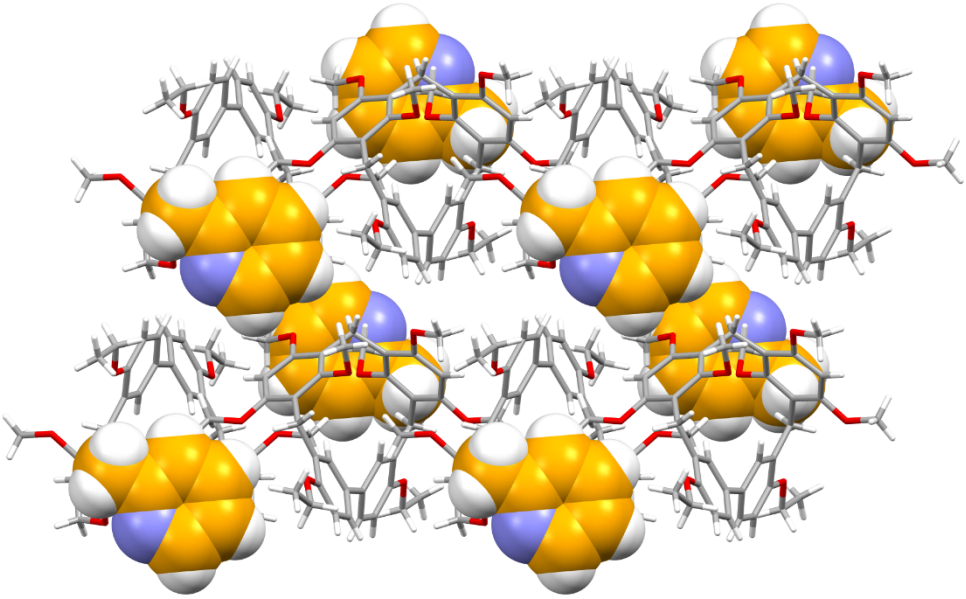

Figure S13. Single crystal structure of **2-PC@H** along *b* axis.

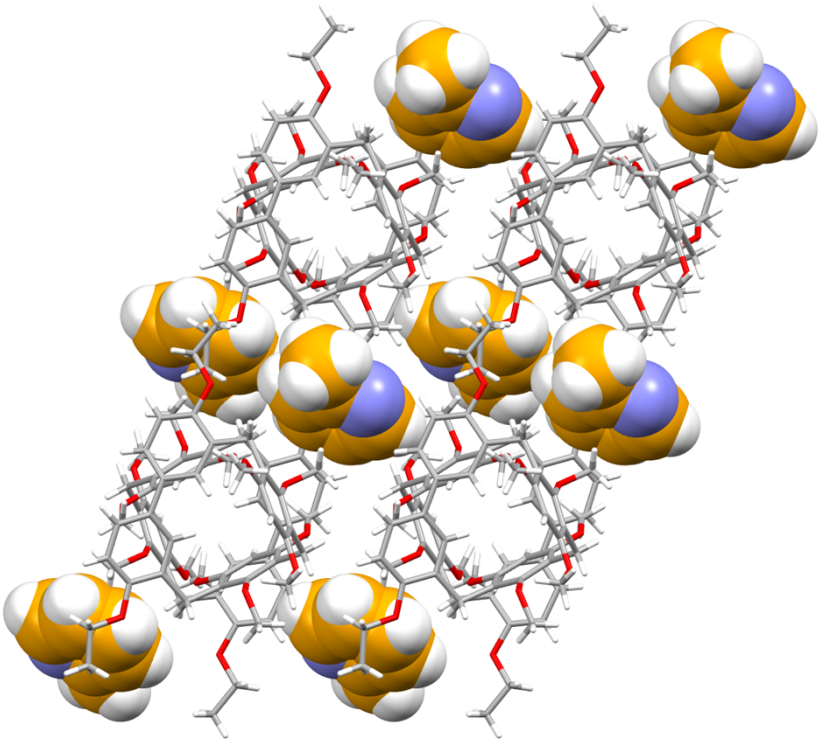

Figure S14. Single crystal structure of **2-PC@H** along *c* axis.

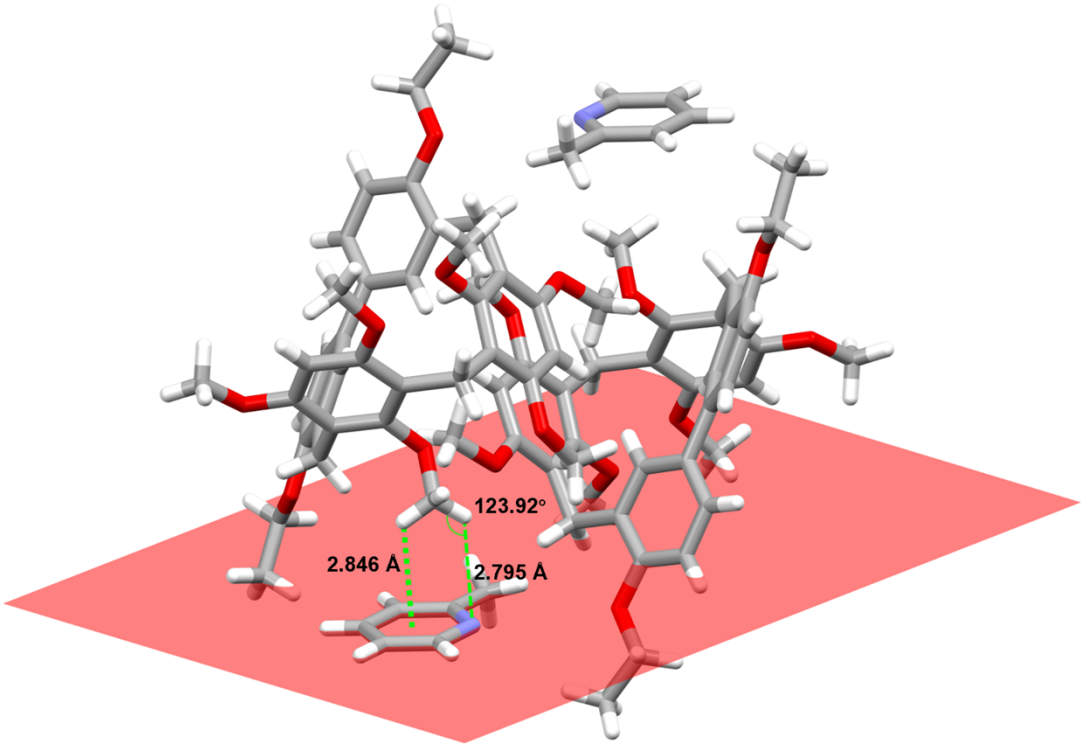

Figure S15. C−H···π and C−H···N interactions between **H** and **2-PC**. C−H···π distance: 2.846 Å; C−H···N distance: 2.795 Å; C−H···N angle: 123.92°.

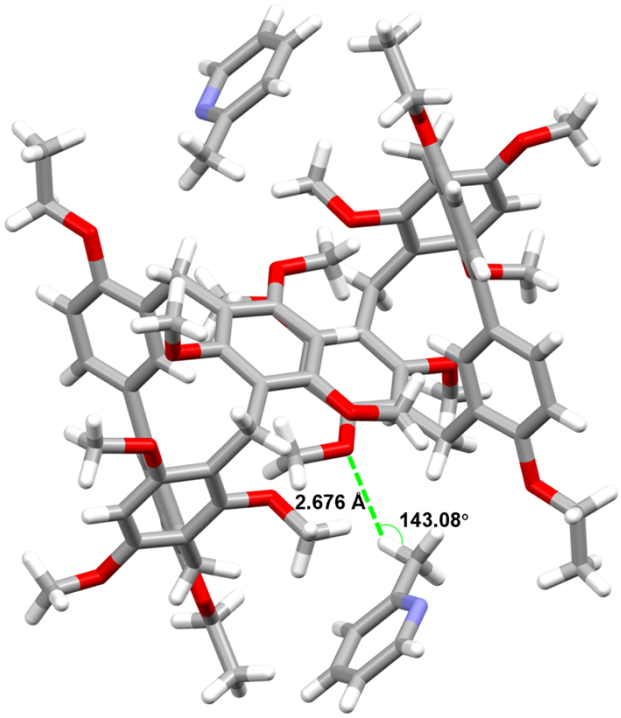

Figure S16. C−H···O interaction between **H** and **2-PC**. C−H···O distance: 2.676 Å; C−H···O angle: 143.08°.

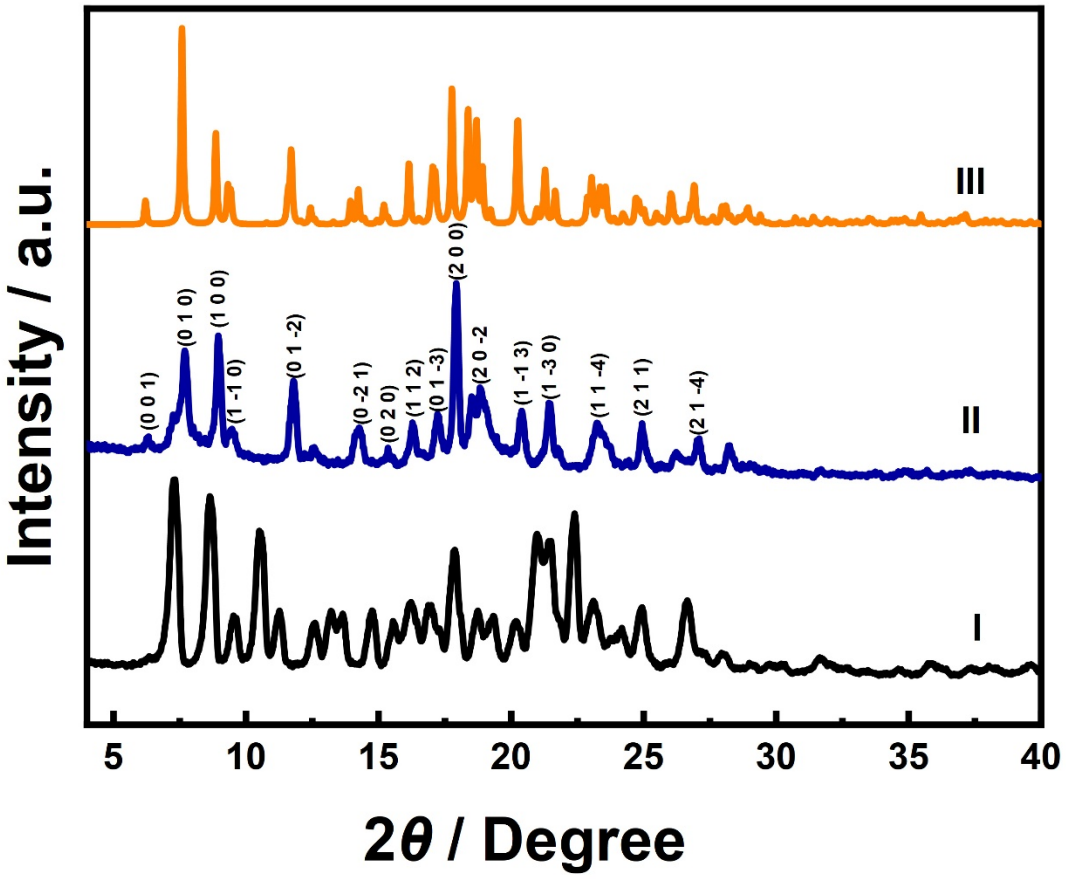

Figure S17. Powder X-ray diffraction patterns of **H***α*: (I) original **H***α*; (II) **H***α* after adsorption of **2-PC**; (III) simulated from the single crystal structure of **2-PC@H**.

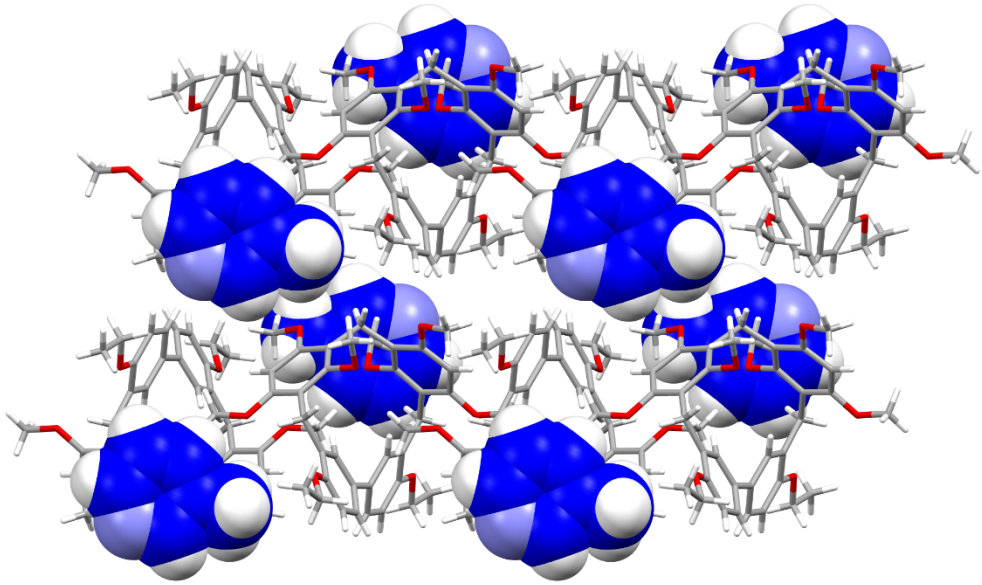

Figure S18. Single crystal structure of **3-PC@H** along *b* axis.

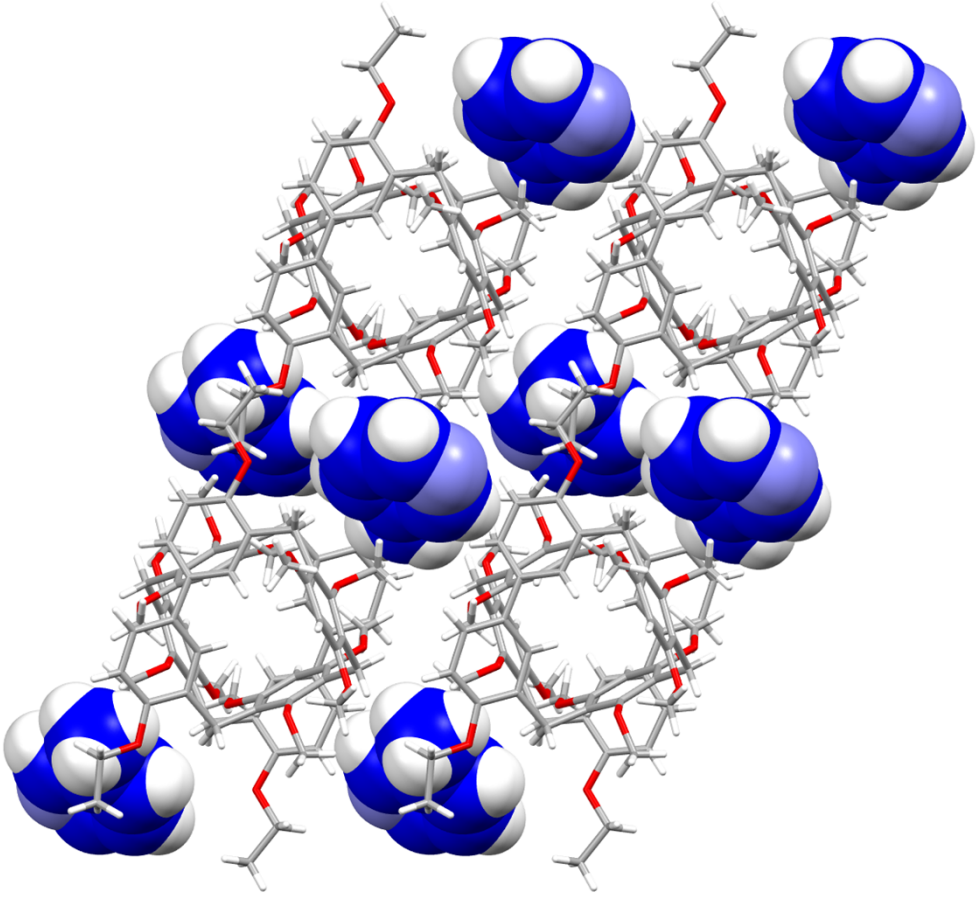

Figure S19. Single crystal structure of **3-PC@H** along *c* axis.

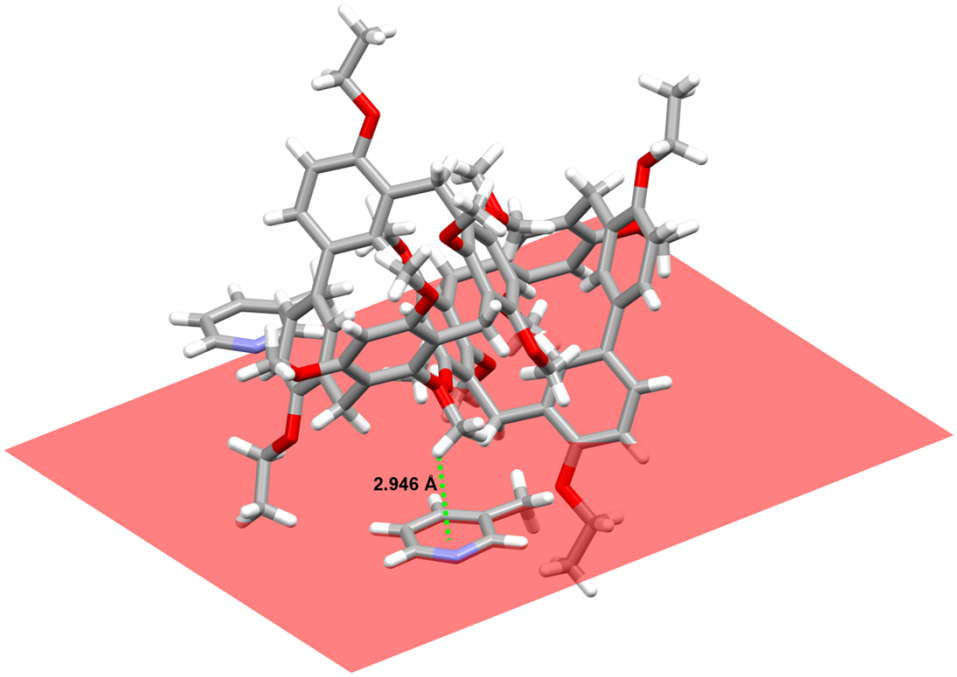

Figure S20. C−H···π interaction between **H** and **3-PC**. C−H···π distance: 2.946 Å.

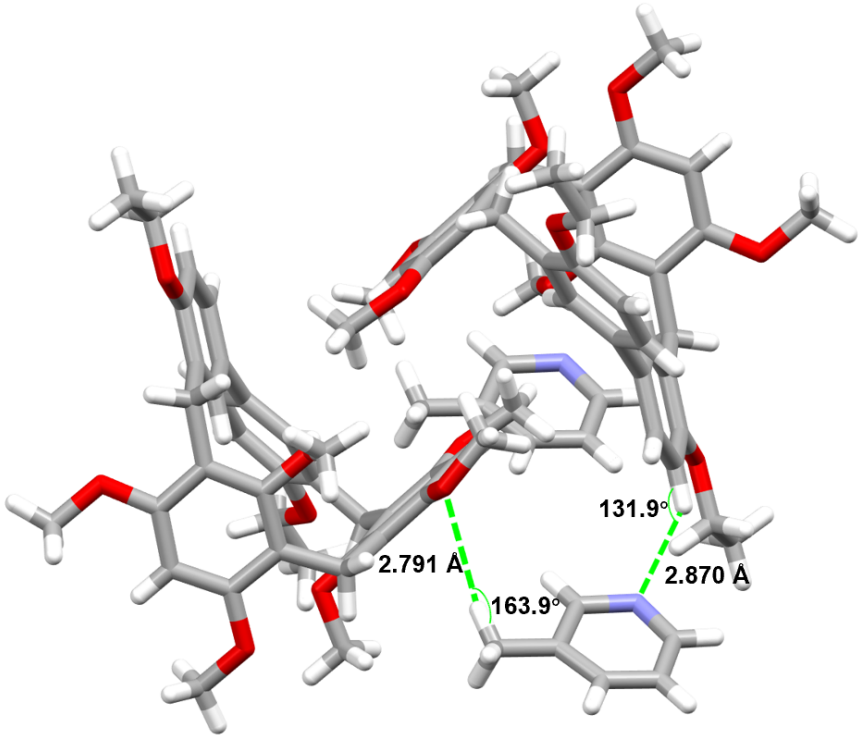

Figure S21. C–H···O and C–H···N interactions between **H** and **3-PC**. C–H···O distance: 2.791 Å; C–H···O angle: 163.9°; C–H···N distance: 2.870 Å; C–H···N angle: 131.9°.

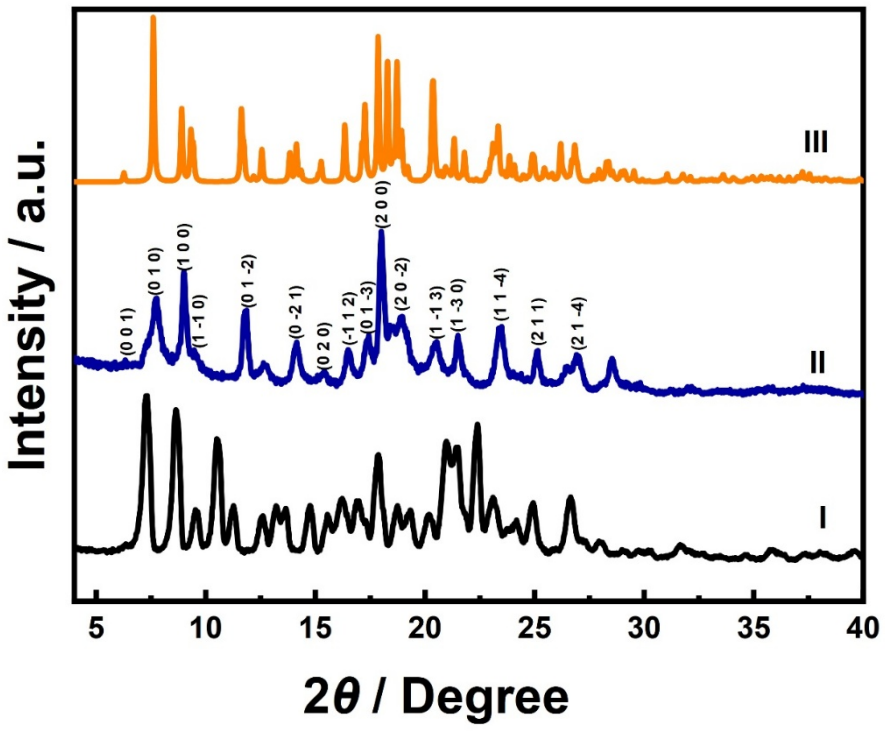

Figure S22. Powder X-ray diffraction patterns of **H***α*: (I) original **H***α*; (II) **H***α* after adsorption of **3-PC**; (III) simulated from the single crystal structure of **3-PC@H**.

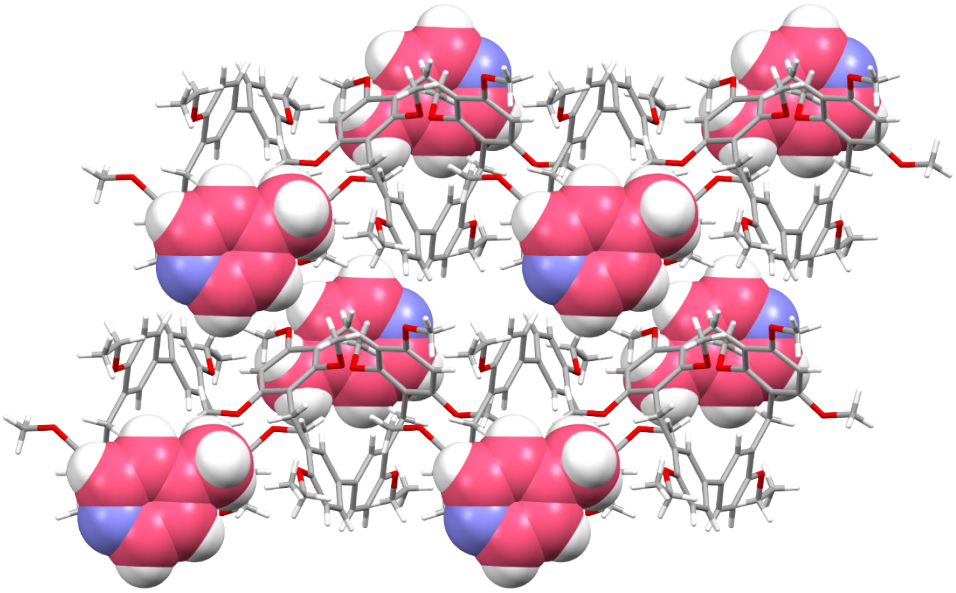

Figure S23. Single crystal structure of **4-PC@H** along *b* axis.

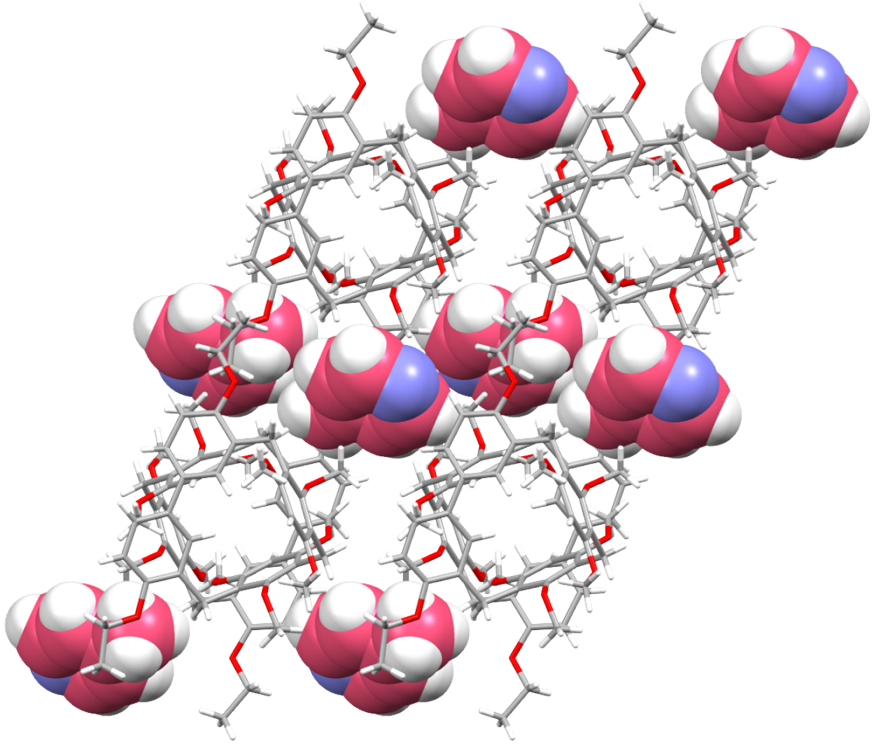

Figure S24. Single crystal structure of **4-PC@H** along *c* axis.

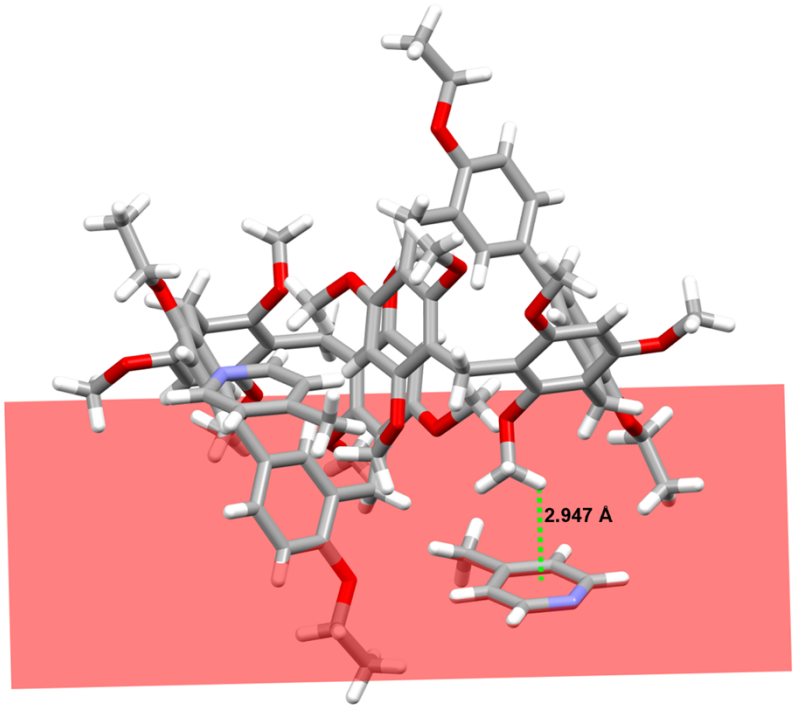

Figure S25. C−H···π interaction between **H** and **4-PC**. C−H···π distance: 2.947 Å.

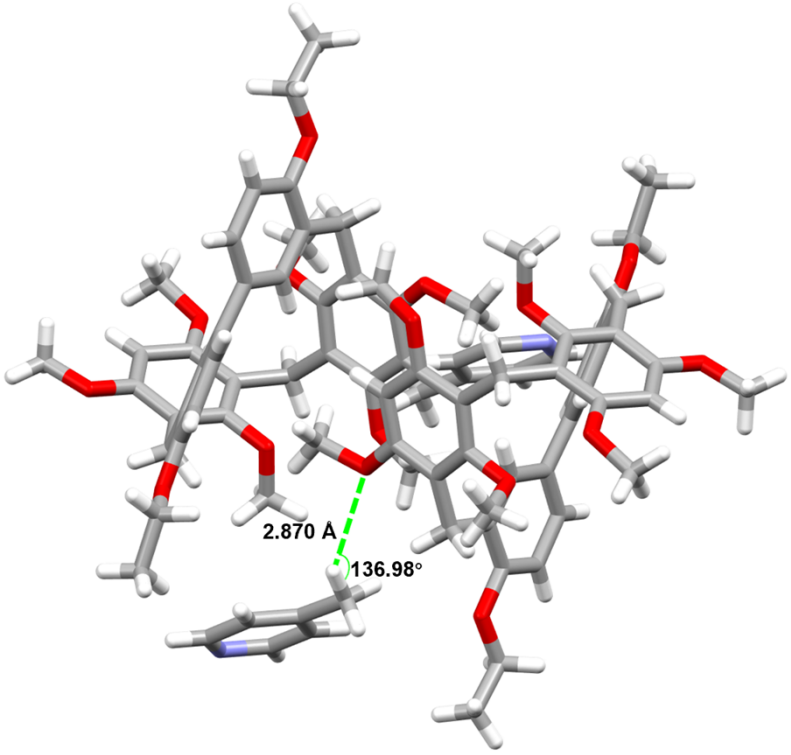

Figure S26. C−H···O interaction between **H** and **4-PC**. C−H···O distance: 2.870 Å; C−H···O angle: 136.98°.

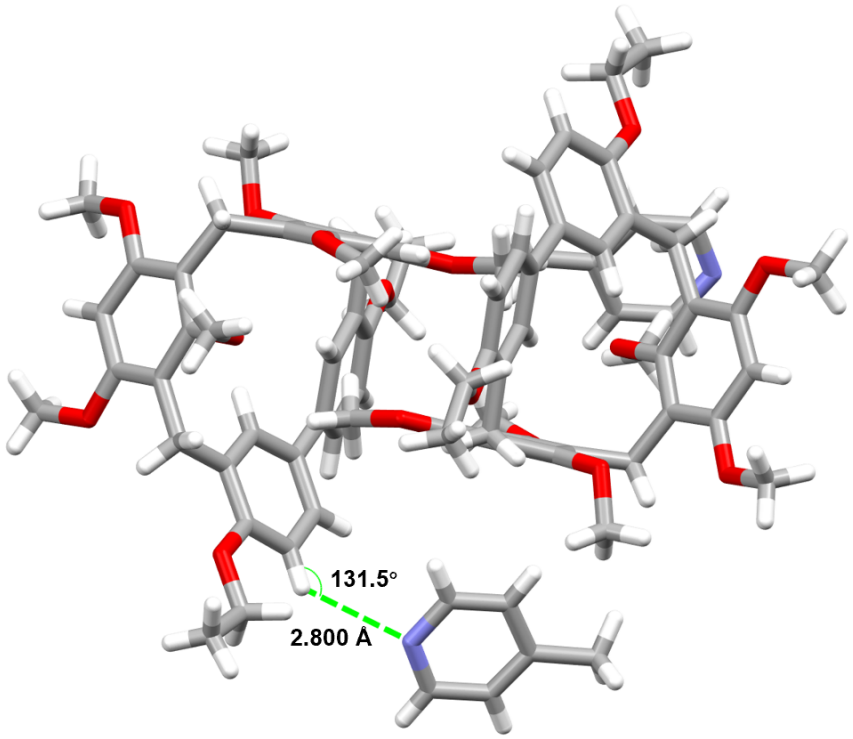

Figure S27. C−H···N interaction between **H** and **4-PC**. C−H···N distance: 2.800 Å; C−H···N angle: 131.5°.

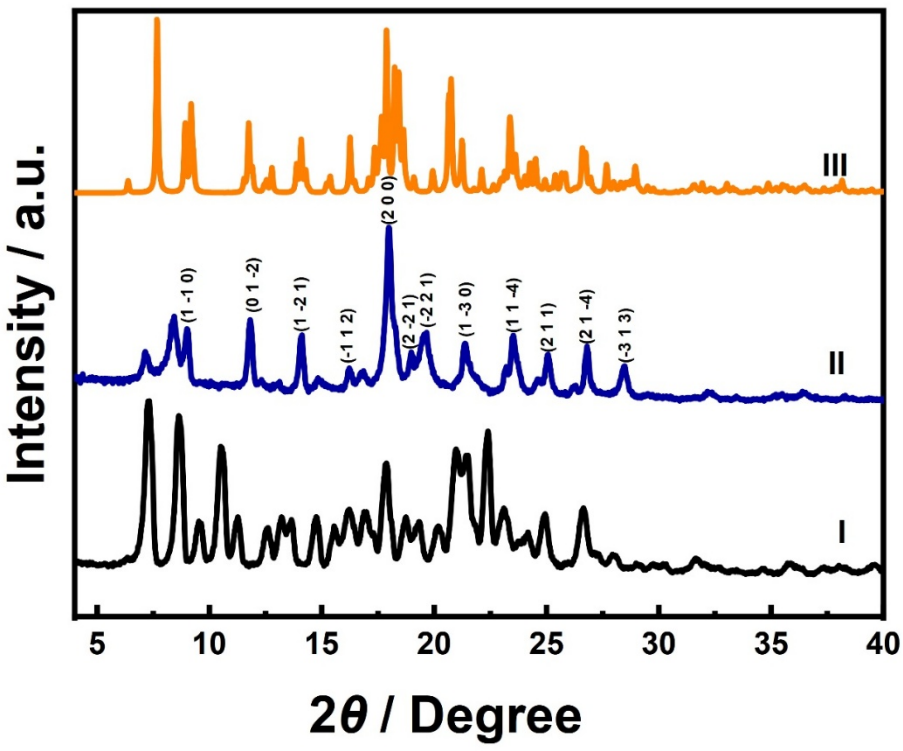

Figure S28. Powder X-ray diffraction patterns of **H***α*: (I) original **H***α*; (II) **H***α* after adsorption of **4-PC**; (III) simulated from the single crystal structure of **4-PC@H**.

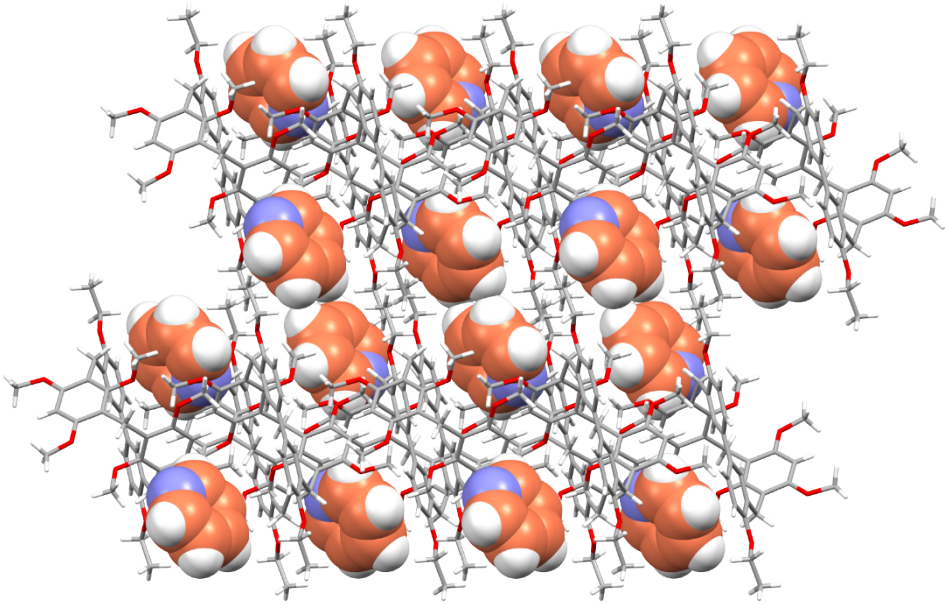

Figure S29. Single crystal structure of **Py@H** along *b* axis.

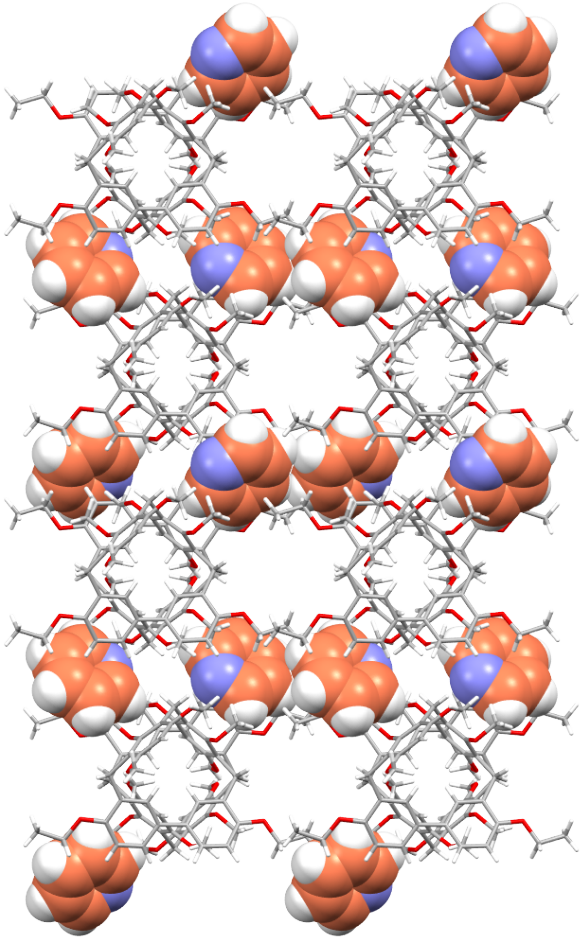

Figure S30. Single crystal structure of **Py@H** along *c* axis.

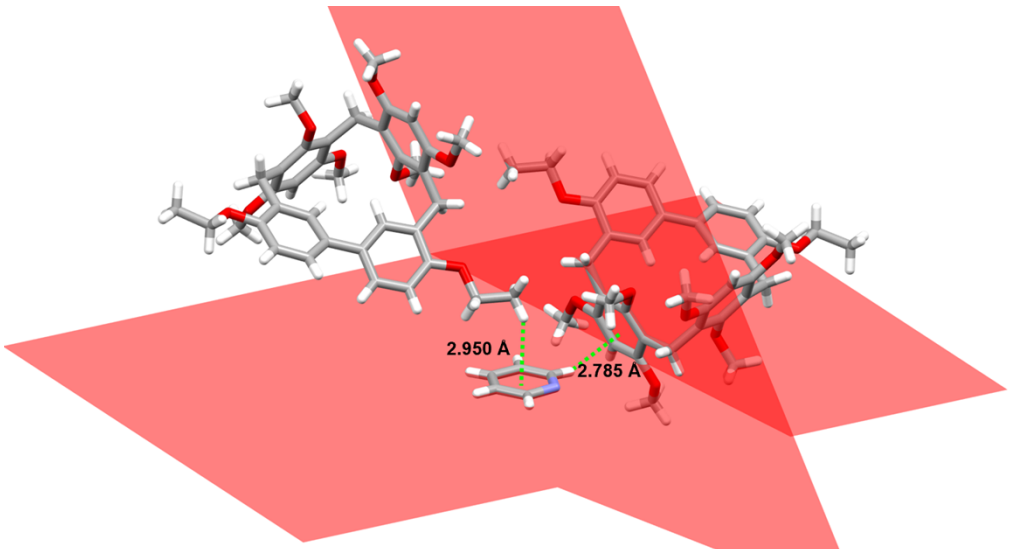

Figure S31. C−H···π interaction between **H** and **Py**. C−H···π distances: 2.950 Å, 2.785 Å.

*7. Selectivity adsorption experiments of **H**α for a **2-PC/Py** mixture (1:1, v/v)*

An open 5 mL vial containing 2.00 mg of guest-free **H***α* adsorbent was placed in a sealed 20 mL vial containing 1 mL of a mixture of **2-PC**/**Py** (1:1, *v*/*v*). Time-dependent solid–vapor adsorption plots of **H***α* were measured by completely dissolving the crystals and measuring the molar ratio of **2-PC** or **Py** to **H** by ^{1}H NMR. Thermogravimetric analysis experiments were performed using **H***α* after adsorption of a mixture of **2-PC**/**Py** for 24 h. The relative uptakes of **2-PC** or **Py** by **H***α* were measured by heating to release the adsorbed vapor and detecting the relative amounts of **2-PC** and **Py** in the released vapor using head space gas chromatography.

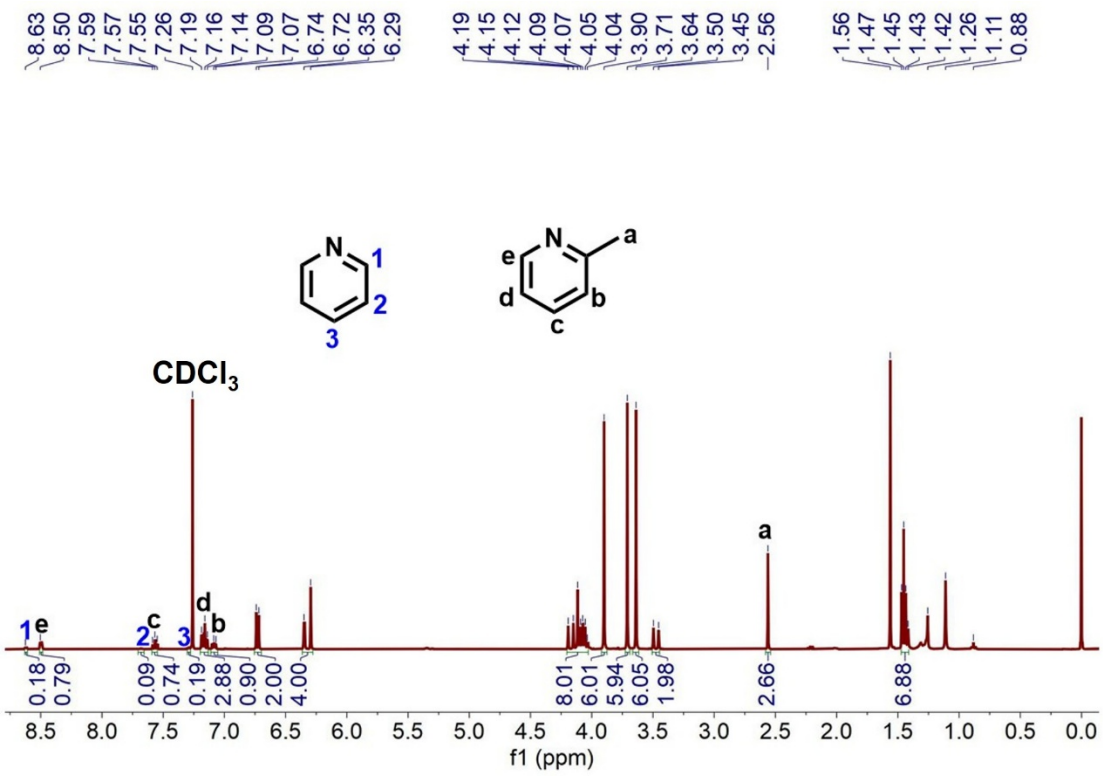

Figure S32. ^{1}H NMR spectrum (400 MHz, $CDCl_3$, 298 K) of **H***α* after adsorption of a mixture of **2-PC**/**Py** (1:1, *v*/*v*) for 24 h.

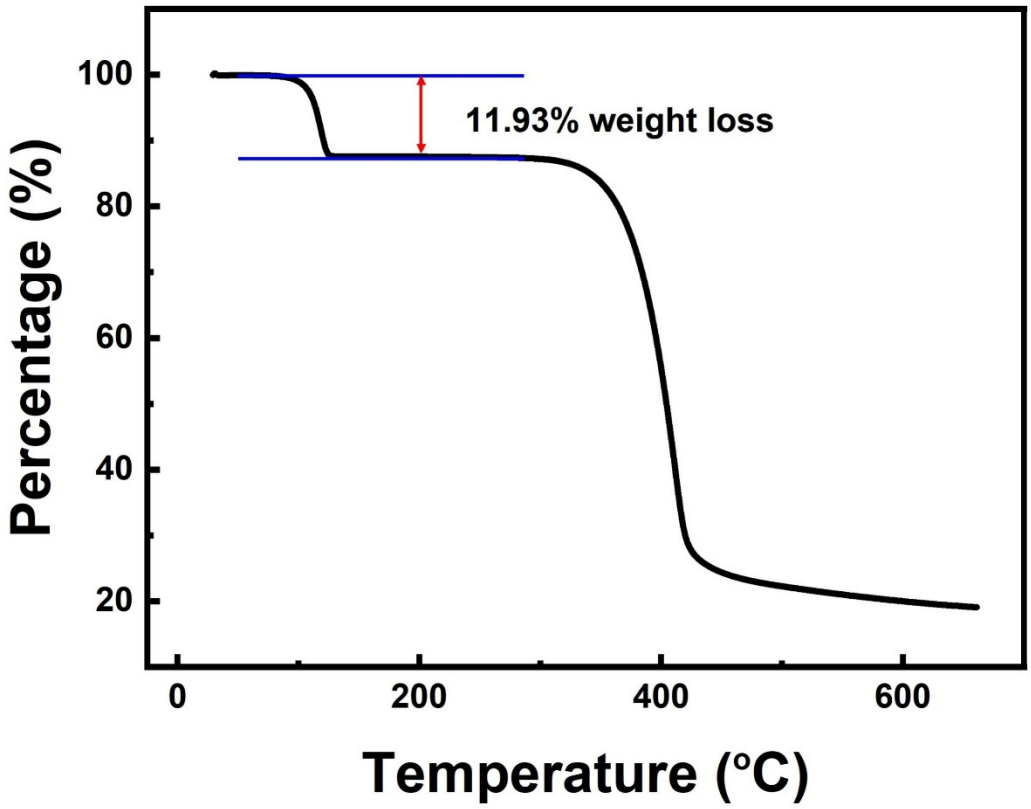

Figure S33. Thermogravimetric analysis of **H***α* after adsorption of a mixture of **2-PC**/**Py** for 24 h. The weight loss below 120 °C can be calculated as 0.89 **2-PC** molecule per **H***α* molecule.

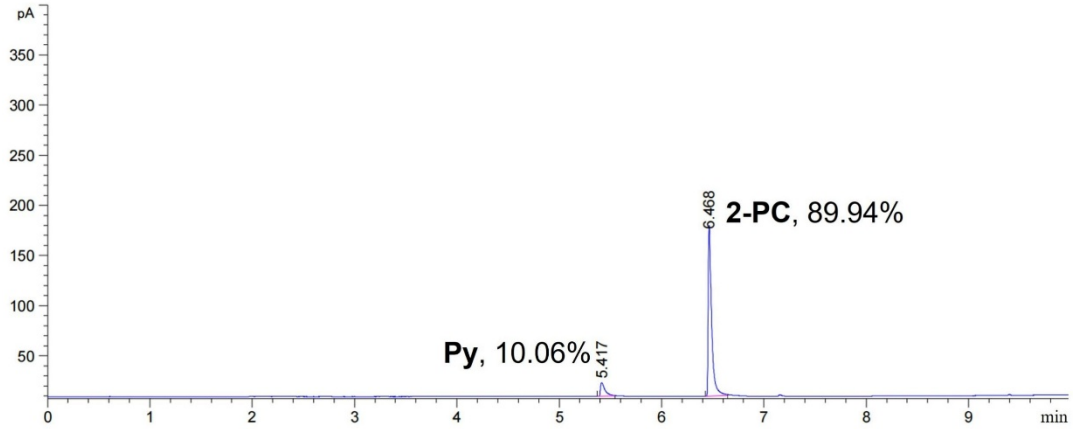

Figure S34. Relative uptakes of **2-PC**/**Py** (1:1, *v*/*v*) by **H***α* for 24 h using head space gas chromatography.

*8. Selectivity adsorption experiments of **Hα** for a **3-PC/Py** mixture (1:1, v/v)*

An open 5 mL vial containing 2.00 mg of guest-free **Hα** adsorbent was placed in a sealed 20 mL vial containing 1 mL of a mixture of **3-PC**/**Py** (1:1, *v*/*v*). Time-dependent solid–vapor adsorption plots of **Hα** were measured by completely dissolving the crystals and measuring the molar ratio of **3-PC** or **Py** to **H** by ^{1}H NMR. Thermogravimetric analysis experiments were performed using **Hα** after adsorption of a mixture of **3-PC**/**Py** for 24 h. The relative uptakes of **3-PC** or **Py** by **Hα** were measured by heating to release the adsorbed vapor and detecting the relative amounts of **3-PC** and **Py** in the released vapor using head space gas chromatography.

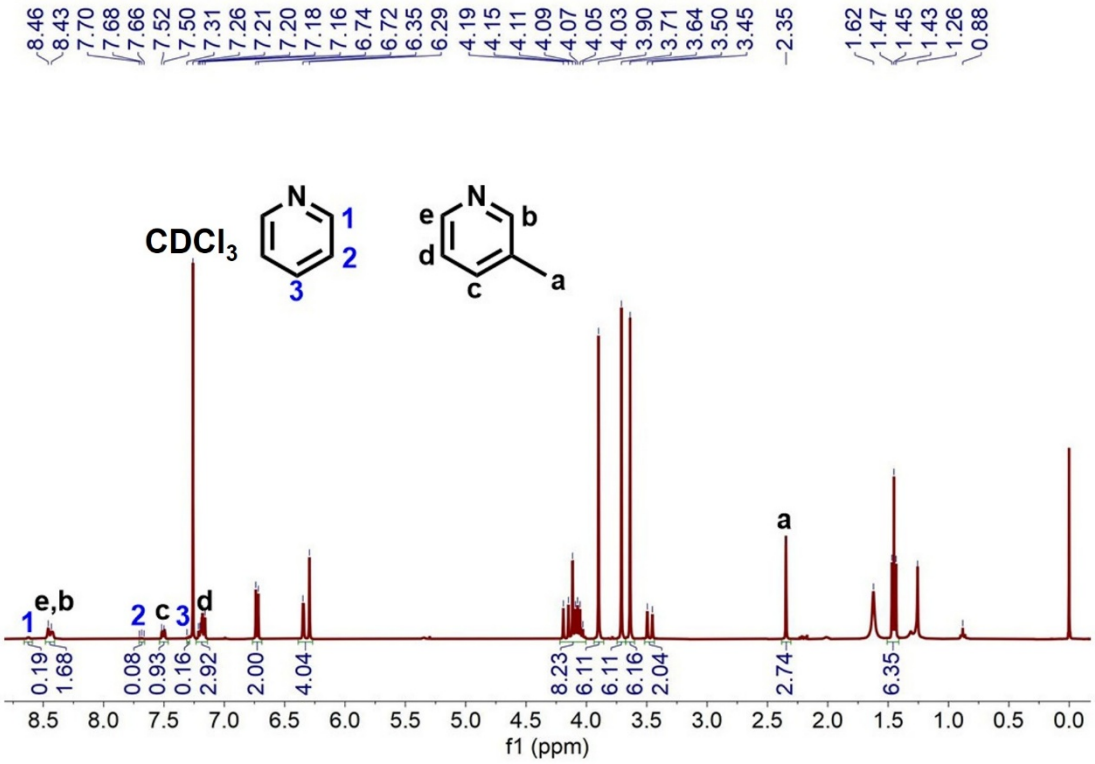

Figure S35. ^{1}H NMR spectrum (400 MHz, $CDCl_3$, 298 K) of **Hα** after adsorption of a mixture of **3-PC**/**Py** (1:1, *v*/*v*) for 32 h.

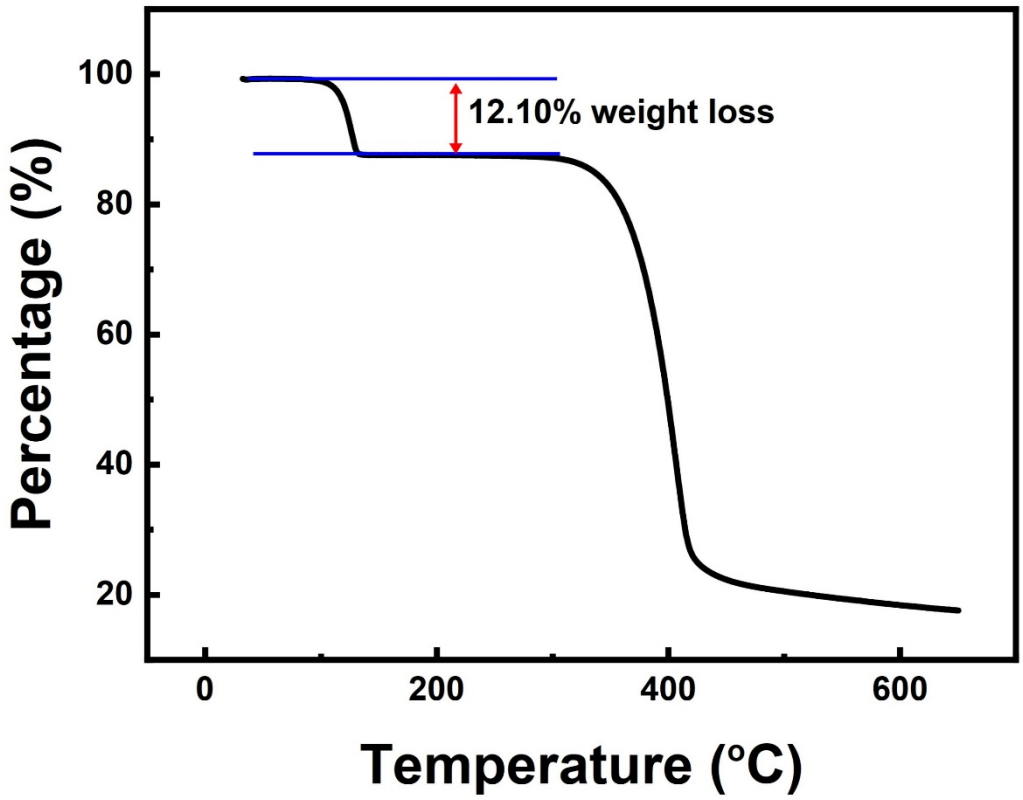

Figure S36. Thermogravimetric analysis of **H***α* after adsorption of a mixture of **3-PC**/**Py** (1:1, *v*/*v*) for 32 h. The weight loss below 150 °C can be calculated as 0.91 **3-PC** molecule per **H***α* molecule.

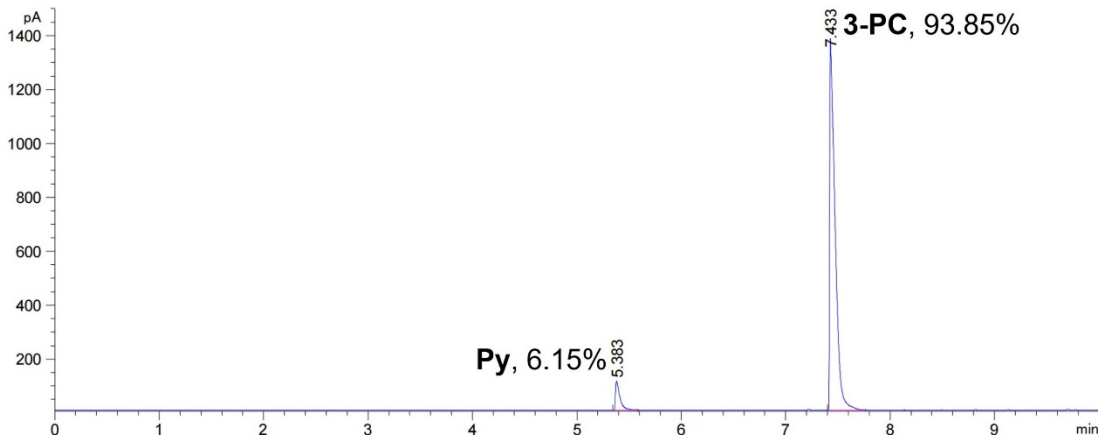

Figure S37. Relative uptakes of **3-PC**/**Py** (1:1, *v*/*v*) by **H***α* for 32 h using head space gas chromatography.

*9. Selectivity adsorption experiments of **Hα** for a of **4-PC**/**Py** mixture (1:1, v/v)*

An open 5 mL vial containing 2.00 mg of guest-free **Hα** adsorbent was placed in a sealed 20 mL vial containing 1 mL of a mixture of **4-PC**/**Py** (1:1, *v*/*v*). Time-dependent solid–vapor adsorption plots of **Hα** were measured by completely dissolving the crystals and measuring the molar ratio of **4-PC** or **Py** to **H** by ^{1}H NMR. Thermogravimetric analysis experiments were performed using **Hα** after adsorption of a mixture of **4-PC**/**Py** for 24 h. The relative uptakes of **4-PC** or **Py** by **Hα** were measured by heating to release the adsorbed vapor and detecting the relative amounts of **4-PC** and **Py** in the released vapor using head space gas chromatography.

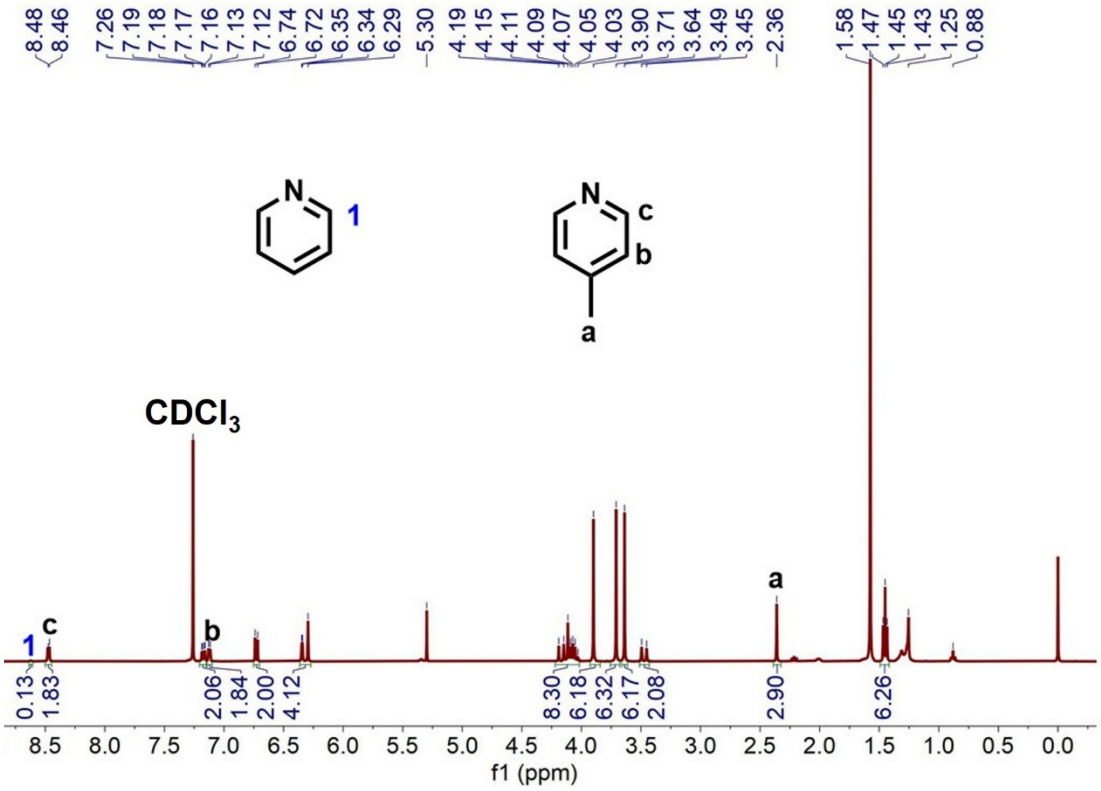

Figure S38. ^{1}H NMR spectrum (400 MHz, $CDCl_3$, 298 K) of **Hα** after adsorption of a mixture of **4-PC**/**Py** (1:1, *v*/*v*) for 12 h.

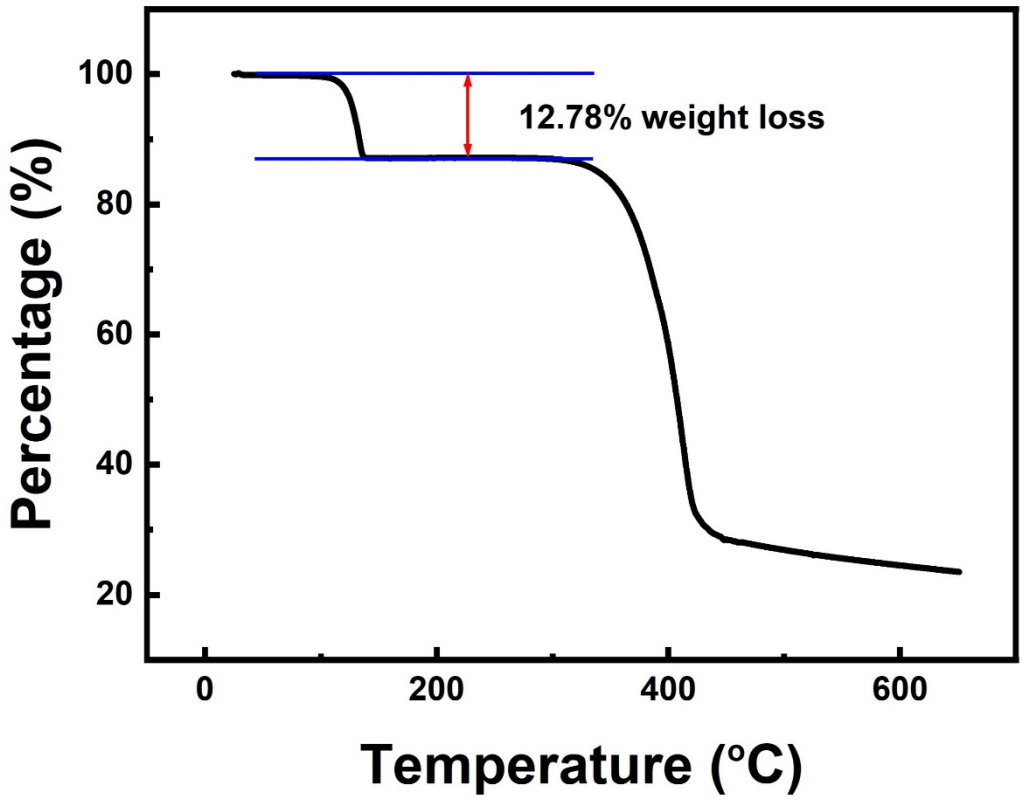

Figure S39. Thermogravimetric analysis of **H***α* after adsorption of a mixture of **4-PC**/**Py** (1:1, *v*/*v*) for 12 h. The weight loss below 120 °C can be calculated as 0.97 **4-PC** molecule per **H***α* molecule.

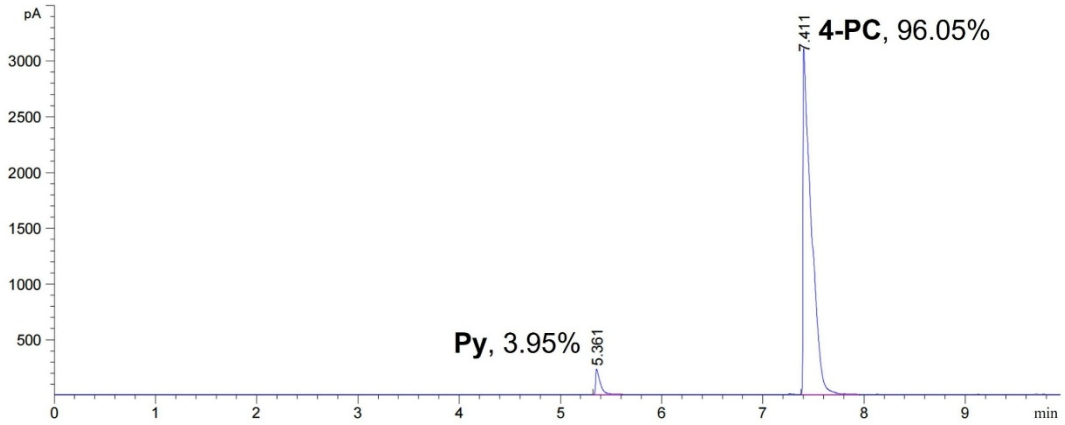

Figure S40. Relative uptakes of **4-PC**/**Py** (1:1, *v*/*v*) by **H***α* for 12 h using head space gas chromatography.

*10. Selectivity adsorption experiments of **H**α for a four-component mixture of **2-PC**, **3-PC**, **4-PC**, and **Py** (1:1:1:1, v/v/v/v)*

An open 5 mL vial containing 2.00 mg of guest-free **H**α adsorbent was placed in a sealed 20 mL vial containing 1 mL of a mixture of **2-PC**/**3-PC**/**4-PC**/**Py** (1:1:1:1, *v*/*v*/*v*/*v*). The molar ratio of **2-PC**, **3-PC**, **4-PC** or **Py** to **H** was measured by ^{1}H NMR. The relative uptakes of **2-PC**, **3-PC**, **4-PC** or **Py** by **H**α were measured by heating to release the adsorbed vapor and detecting the relative amounts of **2-PC**, **3-PC**, **4-PC** and **Py** in the released vapor using head space gas chromatography.

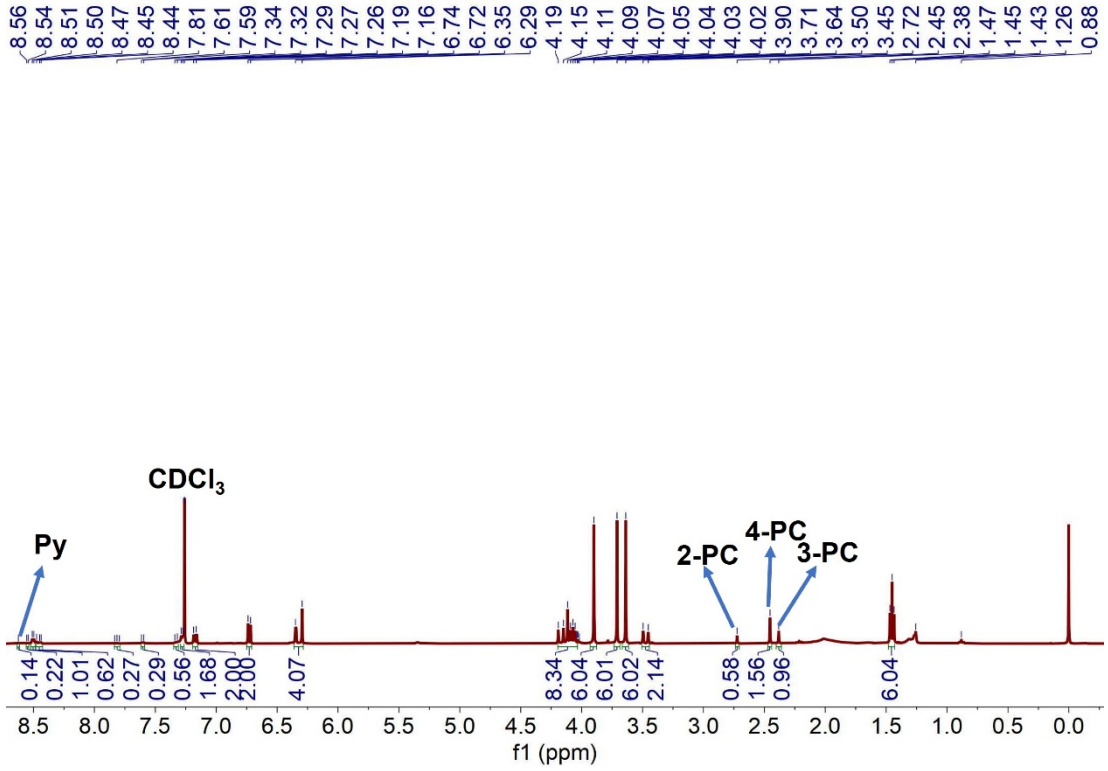

Figure S41. ^{1}H NMR spectrum (400 MHz, $CDCl_3$, 298 K) of **H**α after adsorption of a mixture of **2-PC**/**3-PC**/**4-PC**/**Py** (1:1:1:1, *v*/*v*/*v*/*v*) for 72 h.

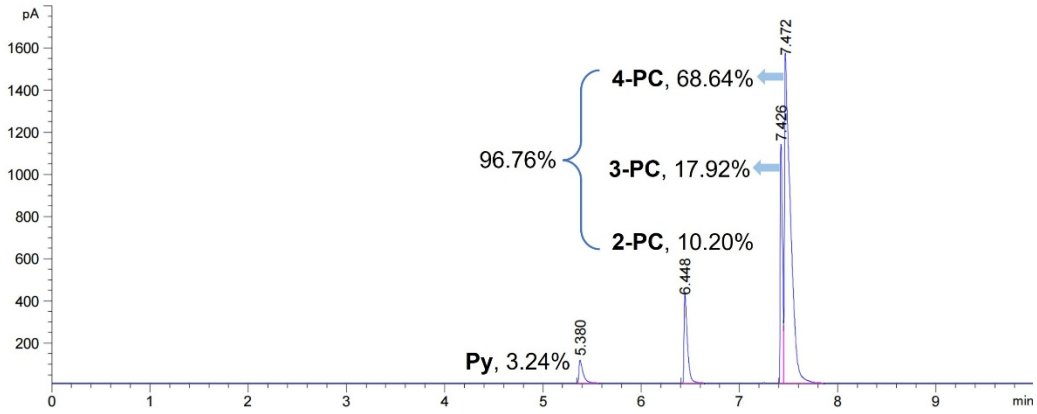

Figure S42. Relative uptakes of **2-PC**/**3-PC**/**4-PC**/**Py** (1:1:1:1, *v*/*v*/*v*/*v*) by **H***α* for 72 h using head space gas chromatography.

*11. Recyclability of **H**α*

An open 5 mL vial containing 20.0 mg of **2-PC@H** was desolvated under vacuum at 150 °C overnight. The resultant crystals were characterized by PXRD and ^{1}H NMR.

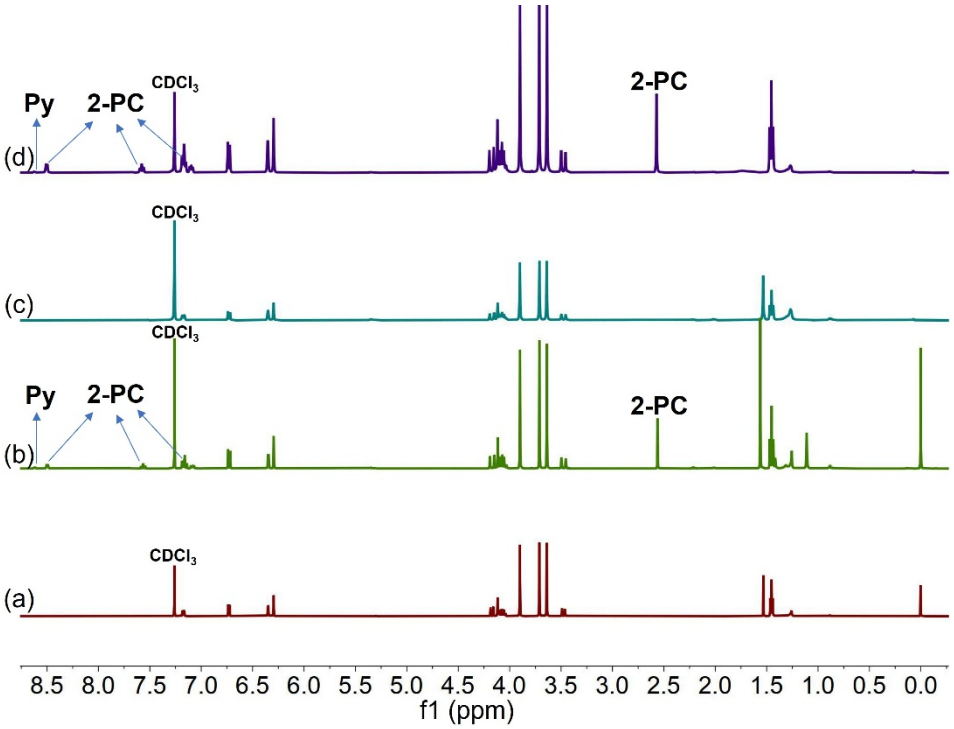

Figure S43. ^{1}H NMR spectra (400 MHz, $CDCl_3$, 298 K): (a) original **H***α*; (b) **H***α* after adsorption of a mixture of **2-PC**/**Py** (1:1, *v*/*v*) for the first cycle; (c) **H***α* after desorption for the tenth cycle; (d) **H***α* after adsorption of a mixture of **2-PC**/**Py** (1:1, *v*/*v*) for the tenth cycle.

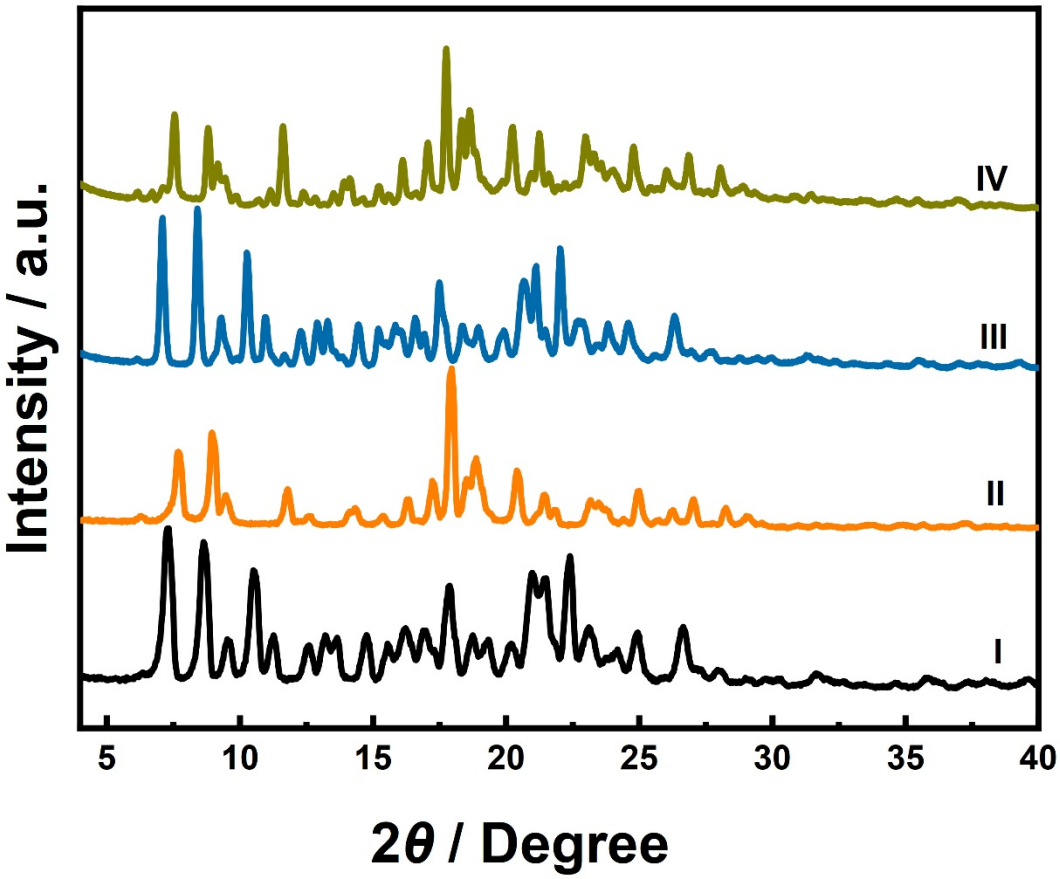

Figure S44. Powder X-ray diffraction patterns of **H***α*: (I) original **H***α*; (II) **H***α* after adsorption of a mixture of **2-PC**/**Py** (1:1, *v*/*v*) for the first cycle; (III) **H***α* after desorption for the tenth cycle; (IV) **H***α* after adsorption of a mixture of **2-PC**/**Py** (1:1, *v*/*v*) for the tenth cycle.

An open 5 mL vial containing 20 mg of **3-PC@H** was desolvated under vacuum at 150 ℃ for 12 h. The resultant crystals were characterized by PXRD and ^{1}H NMR.

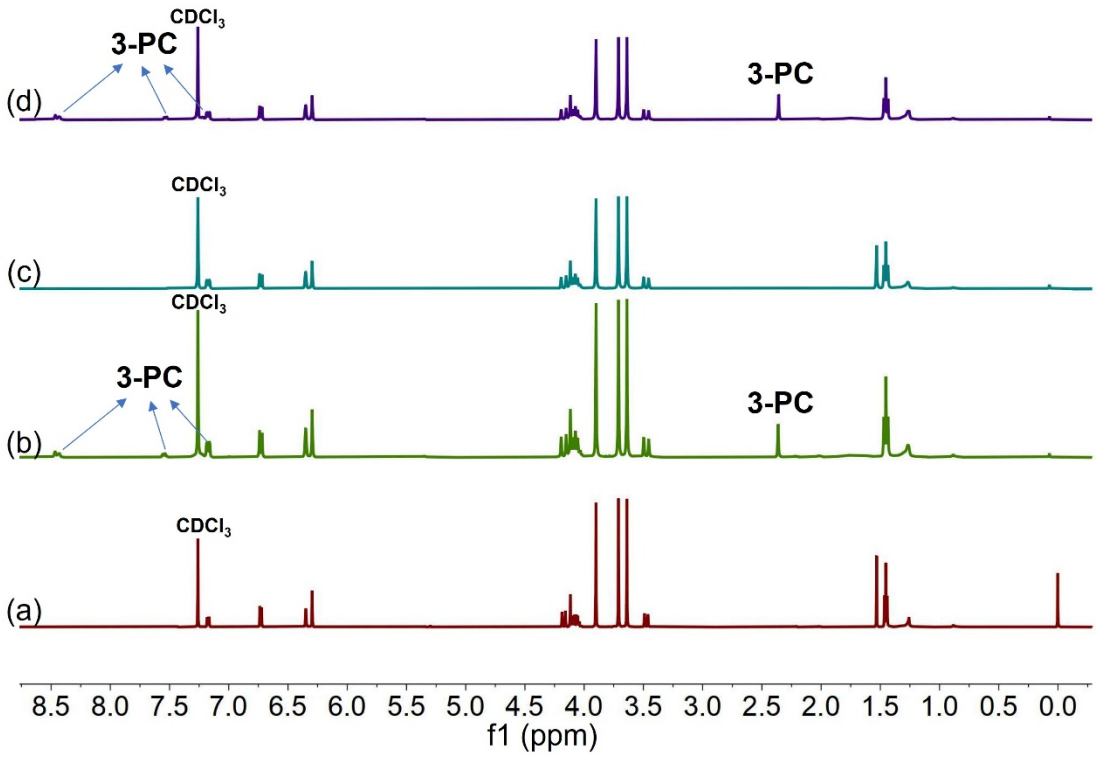

Figure S45. ^{1}H NMR spectra (400 MHz, $CDCl_3$, 298 K): (a) original **H***α*; (b) **H***α* after adsorption of a mixture of **3-PC**/**Py** (1:1, *v*/*v*) for the first cycle; (c) **H***α* after desorption for the tenth cycle; (d) **H***α* after adsorption of a mixture of **3-PC**/**Py** (1:1, *v*/*v*) for the tenth cycle.

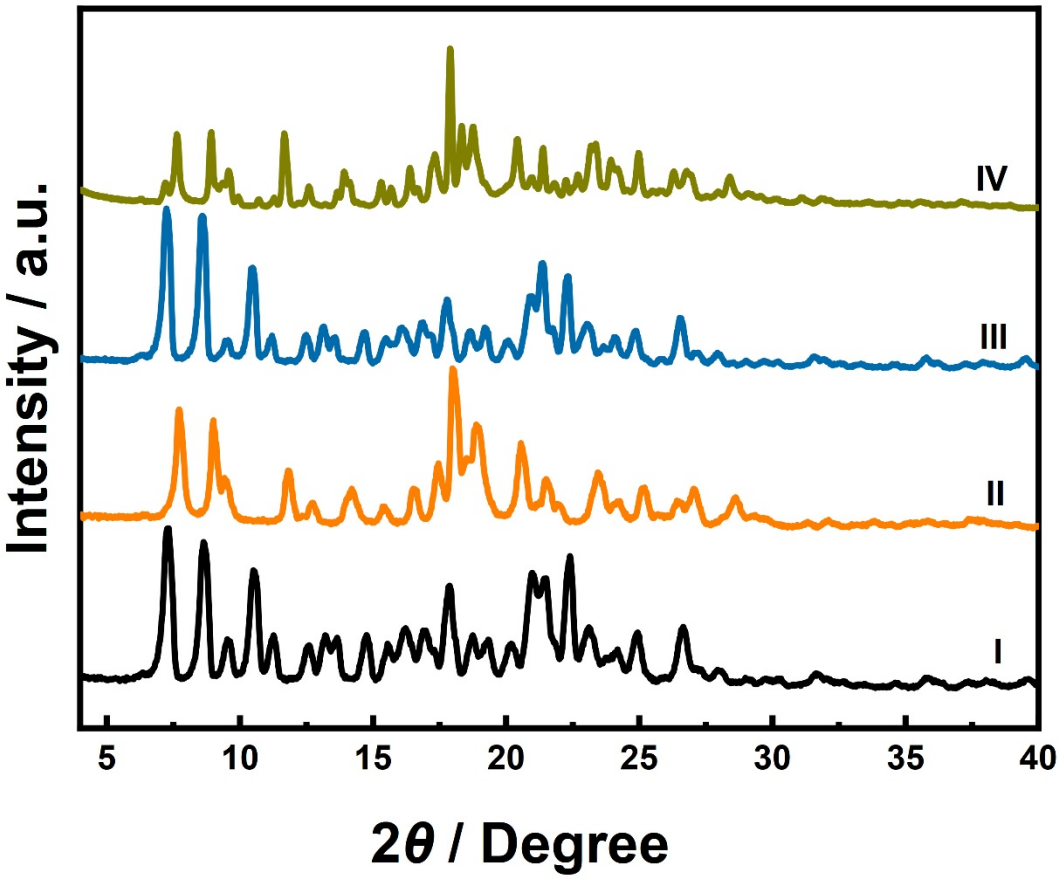

Figure S46. Powder X-ray diffraction patterns of **H***α*: (I) original **H***α*; (II) **H***α* after adsorption of a mixture of **3-PC**/**Py** (1:1, *v*/*v*) for the first cycle; (III) **H***α* after desorption for the tenth cycle; (IV) **H***α* after adsorption of a mixture of **3-PC**/**Py** (1:1, *v*/*v*) for the tenth cycle.

An open 5 mL vial containing 20.0 mg of **4-PC@H** was desolvated under vacuum at 150 °C for 12 h. The resultant crystals were characterized by PXRD and ^{1}H NMR.

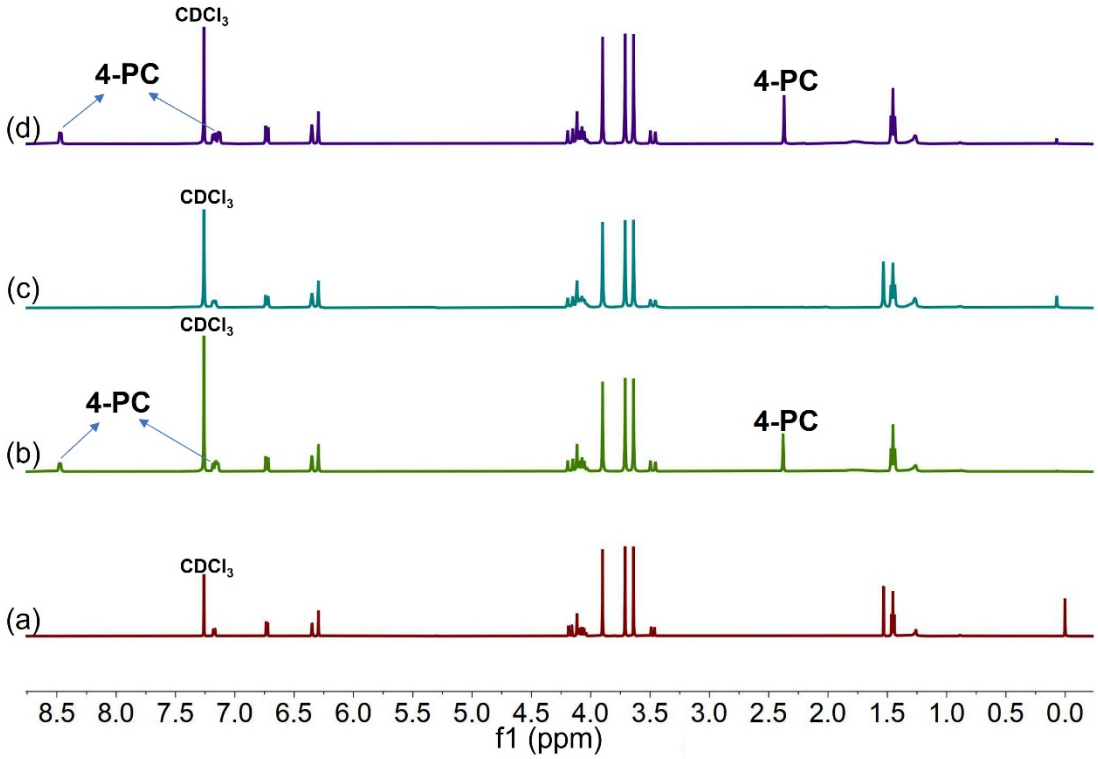

Figure S47. ^{1}H NMR spectra (400 MHz, $CDCl_3$, 298 K): (a) original **H***α*; (b) **H***α* after adsorption of a mixture of **4-PC**/**Py** (1:1, *v*/*v*) for the first cycle; (c) **H***α* after desorption for the tenth cycle; (d) **H***α* after adsorption of a mixture of **4-PC**/**Py** (1:1, *v*/*v*) for the tenth cycle.

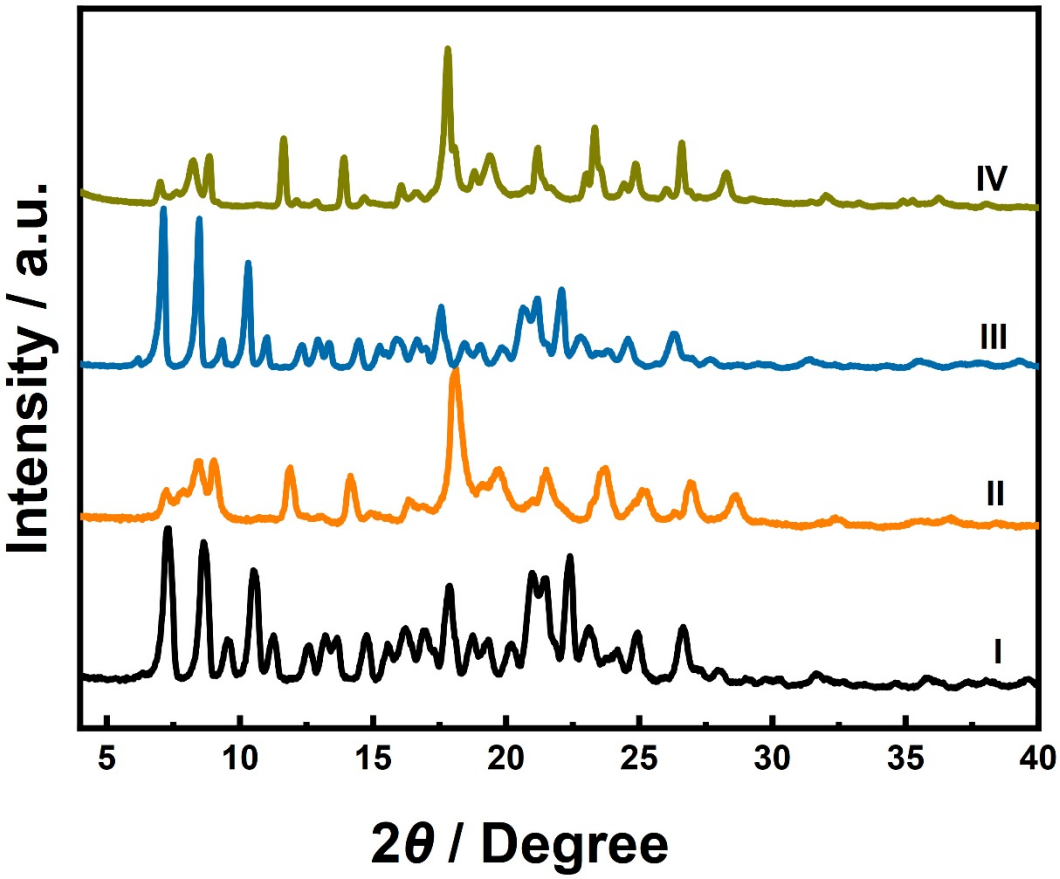

Figure S48. Powder X-ray diffraction patterns of **H***α*: (I) original **H***α*; (II) **H***α* after adsorption of a mixture of **4-PC**/**Py** (1:1, *v*/*v*) for the first cycle; (III) **H***α* after desorption for the tenth cycle; (IV) **H***α* after adsorption of a mixture of **4-PC**/**Py** (1:1, *v*/*v*) for the tenth cycle.

12. Advantages and disadvantages of selectively adsorbing materials

Table S3 Comparison of adsorptive properties of **H***α* with reported typical adsorbing materials.

Adsorbing materials		**Advantages**	**Disadvantages**	Refs.
Metal–organic frameworks	ZJU-520(Al) Zn-hba MOF-5	Unprecedented tunability; ultrahigh specific surface area and porosity; diverse adsorption sites	Limited stability; high synthesis cost; challenges in shaping and recovery	9–11
Covalent organic frameworks	TAPB-PDA-COF COF-300 PI-COF	High structural designability; large specific surface area; excellent thermal and chemical stability	High synthesis cost and difficulty; insufficient water stability; difficulty in scalable preparation	12–14
Porous organic cages	CC3 RCC3 CPOC-107	High porosity and specific surface area; facile pore structure tunability; high solution processability	Insufficient chemical stability; difficult post-synthetic structural regulation; limitations in large-scale synthesis	15–17
Nonporous adaptive crystals	EtP5*α* Q[6] **H***α*	Low energy consumption; high chemical and thermal stability; excellent recyclability	Poor solution processability; lack of permanent porosity; sensitive to acidic/alkaline environments	2, 18, 19

13. References

1. J. Zhou, J. Yang, B. Hua, L. Shao, Z. Zhang and G. Yu, The synthesis, structure, and molecular recognition properties of a [2]calix[1]biphenyl-type hybrid[3]arene, *Chem. Commun.*, 2016, **52**, 1622–1624.

2. J. Zhou, G. Yu, Q. Li, M. Wang and F. Huang, Separation of Benzene and Cyclohexane by Nonporous Adaptive Crystals of a Hybrid[3]arene, *J. Am. Chem. Soc.*, 2020, **142**, 2228–2232.

3. F. Weigend and R. Ahlrichs, Balanced basis sets of split valence, triple zeta valence and quadruple zeta valence quality for H to Rn: Design and assessment of accuracy, *Phys. Chem. Chem. Phys.*, 2005, **7**, 3297–3305.

4. F. Weigend, Accurate Coulomb-fitting basis sets for H to Rn, *Phys. Chem. Chem. Phys.*, 2006, **8**, 1057–1065.

5. F. Neese, Software update: the ORCA program system, version 4.0, *Wires. Comput. Mol. Sci.*, 2018, **8**, e1327.

6. T. Lu and F. Chen, Multiwfn: A multifunctional wavefunction analyzer, *J. Comput. Chem.*, 2012, **33**, 580–592.

7. T. Lu and Q. Chen, Independent gradient model based on Hirshfeld partition: A new method for visual study of interactions in chemical systems, *J. Comput. Chem.*, 2022, **43**, 539–555.

8. T. Lu and Q. Chen, Shermo: A general code for calculating molecular thermochemistry properties, *Comput. Theor. Chem.*, 2021, **1200**, 113249.

9. L. Hu, W. Wu, M. Hu, L. Jiang, D. Lin, J. Wu, K. Yang, Double-walled Al-based MOF with large microporous specific surface area for trace benzene adsorption, *Nat Commun*. 2024, **15**, 3204.

10. Y. Zhang, S. Deng, X. Cui, J. Yue, H. Huang, C. Xue, H. Yang, L. Gan, Scalable synthesis of a low-cost Zn–MOF with a nonpolar pore surface for efficient separation ofmethanol-to-olefin products, *Chem. Sci.*, 2025, **16**, 19381.

11. Y. Wang, Z.-J. Jiang, W. Lu and D. Li, Machine Learning-Assisted Exploration of Chemical Space of MOF-5 Analogs for Enhanced C_2H_6/C_2H_4 Separation, *Angew. Chem. Int. Ed.*, 2025, **64**, e202500783.

12. L. Wu, A. Dou, Q. Miao, D. Chen, Y. Liu, Y. Sui, N. Cao, Z. Zhu and J. Pang, Biomimetic and durable sea grape-like COFs membrane for high performance emulsion separation and dye removal, *J. Hazard. Mater.*, 2025, **499**, 140140.

13. Q. Wang, X. Yang, H. Li, B. Li, B. Li, X. Wang and Z. Wang, Electrostatic potential matching guided ultra-microporous COF-300 for C_2H_2/CO_2 separation with scale-up synthesis, *Chem. Commun.*, 2025, **61**, 13956–13959.

14. H. Zheng, H. Li, J. Ji, F. Chen, Y. Wang, J. Suo, J. Song, D. Zhao, V. Valtchev, S. Qiu and Q. Fang, Topological Derivative Strategy for Large-Pore Three-Dimensional Covalent Organic Frameworks, *J. Am. Chem. Soc*, 2025, **147**, 39223–39231.

15. J. M. Lucero and M. A. Carreon, Separation of Light Gases from Xenon over Porous Organic Cage Membranes, *ACS Appl. Mater. Interfaces*, 2020, **12**, 32182–32188.

16. X. Li, W. Lin, V. Sharma, R. Gorecki, M. Ghosh, B. A. Moosa, S. Aristizabal, S. Hong, N. M. Khashab and S. P. Nunes, Polycage membranes for precise molecular separation and catalysis, *Nat. Commun.*, 2023, **14**, 3112.

17. L. Feng, Y. Xie, W. Wang, K. Su and D. Yuan, Nitrogen-rich porous organic cages with high acetylene storage and separation performance, *J. Mater. Chem. A*, 2023, **11**, 25316–25321.

18. K. Jie, M. Liu, Y. Zhou, M. Little, S. Bonakala, S. Chong, A. Stephenson, L. Chen, F. Huang and A. I. Cooper, Styrene Purification by Guest-Induced Restructuring of Pillar[6]arene, *J. Am. Chem. Soc.*, 2017, **139**, 2908.

19. Q. Li, K. Jie, F. Huang, Highly Selective Separation of Minimum-Boiling Azeotrope Toluene/Pyridine by Nonporous Adaptive Crystals of Cucurbit[6]uril, *Angew. Chem. Int. Ed.*, 2020, **59**, 5355–5358.